Bayesian inference of high-dimensional finite-strain visco-elastic-visco-plastic model parameters for additive manufactured polymers and neural network based material parameters generator

Ling Wu**[a], Cyrielle Anglade[a], Lucia Cobian[c,b], Miguel Monclus[b], Javier Segurado[c,b], Fatma Karayagiz[d], Ubiratan Freitas[d], Ludovic Noels[a]

[a] *University of Liege, Department of Mechanical and Aerospace Engineering, Computational & Multiscale Mechanics of Materials, Allée de la découverte 9, B-4000 Liège, Belgium*
[b] *IMDEA Materials Institute, Calle Eric Kandel 2, Getafe, 28906, Madrid, Spain*
[c] *Universidad Politécnica de Madrid, Department of Materials Science, E.T.S.I. Caminos, 28040, Madrid, Spain*
[d] *cirp GmbH, Römerstraße 8, 71296, Heimsheim, Germany*
Preprint submitted to International Journal of Solids and Structures. (C) 2023; Licensed under the Creative Commons (CC-BY-NC-ND); formal publication on: 10.1016/j.ijsolstr.2023.112470

Abstract

In this work, the parameters of a finite-strain visco-elastic-visco-plastic formulation with pressure dependency in both the visco-elastic and visco-plastic parts are identified using as observations experimental data obtained from tension and compression tests at different strain rates ranging from $10^{-4}\,\mathrm{s}^{-1}$ to $10^{3}\,\mathrm{s}^{-1}$. Because of the high number of parameters of the model, a sequential Bayesian Inference (SBI) framework with data augmentation, which presents several advantages, is developed. First the sequential nature reduces the difficulty of selecting the appropriate prior distributions by considering only parts of the observations at a time. Second, the sequential nature prevents dealing with low likelihood values by considering only a part of the experimental observations at a time, but also subsets of the material parameters to be identified, improving the convergence of the Markov Chain Monte Carlo (MCMC) random walk. Third, the data augmentation allows considering different number of experimental tests in tension and in compression while preserving the identified model accuracy for both loading modes.

This SBI is carried out to infer the properties of Polyamide 12 (PA12) processed by Selective Laser Sintering (SLS) for two different printing directions and it is shown that the models fed by their respective set of inferred parameters can reproduce the different experimental tests.

Finally, in order for upcoming structural simulations to benefit from the information related to the uncertainties due to the measurement errors, the identification process and the model limitations, we introduce a Generative Adversarial Network (GAN), which is trained using the data obtained from MCMC random walk. This generators can then serve to produce a synthetic data-set of arbitrary size of the material parameters to be used in finite-element simulations.

Keywords: Bayesian inference, Visco-elasticity-visco-plasticity, Selective Laser Sintering, Polyamide,

**Corresponding author: L. Wu; L.Wu@ulg.ac.be; +32 366 96 55

1. Introduction

Selective Laser Sintering (SLS) is a type of industrial Powder Bed Fusion (PBF) process which creates 3D objects by the sintering of powdered materials using infrared laser beams [1]. 3D printing by SLS is a favored manufacturing technique and is widely used in the preparation of polymer and its composites [2]. Laser sintered Polyamide 12 (PA12) is a versatile thermoplastic with excellent properties: this material has low relative density, low water absorption, excellent long-term stability, and is resistant against most chemicals. It also has a low melting point and hence requires low processing temperatures and low laser power [3]. Therefore, it has become the most widely used polymer in the SLS system.

Although SLS of PA12 offers unparalleled design flexibility and is fast and economical for short production runs, creating final parts with layered structures can lead to different strengths in relation to the printing direction and various degrees of porosity, which can lead to various mechanical performance [4, 5]. The process of 3D printing commonly starts with the Computer Aided Design (CAD) conceptualization, followed by numerical analyses, such as finite element simulations, to evaluate the mechanical performance of the final 3D printed polymer parts, which helps to set up the right printing parameters, such as printing direction. However, a valuable computation is based on a reliable assessment of material properties and on the proper choice of the material constitutive model. The mechanical properties of laser sintered PA12 have been studied experimentally by several researchers. Some of them focused on the effects of the thermal history related parameters on the mechanical properties of laser sintered PA12 [6, 7], and on the influence of the printing position and direction [4, 8]. The mechanical experiments have shown that the mechanical properties of PA12 are highly strain rate dependent and that PA12 exhibits a visco-elastic-visco-plastic (VE-VP) behavior [9]. In order to obtain a comprehensive understanding of these VE-VP behaviors, a broad set of mechanical tests, such as tension and compression, has been carried out on the bulk laser sintered PA12 specimens in the work of [10]. On the aspect of material constitutive modeling, the visco-elastic material model has been used to describe the mechanical response of PA12 in [11]. Although the variability of the material parameters is studied in [8], the material is only represented with an elastic constitutive model, while according to the experimental observations, the mechanical behavior of laser sintered PA12 needs to be represented by a complete VE-VP constitutive model, which accounts for pressure dependency effects.

The complex behavior of polymers can be captured using a VE-VP constitutive model [12]. A finite-strain visco-elastic model [13] and visco-plastic model [14] have been combined and reinforced by damage

Email addresses: L.Wu@ulg.ac.be (Ling Wu*), lucia.cobian@imdea.org (Lucia Cobian), miguel.monclus@imdea.org (Miguel Monclus), javier.segurado@imdea.org (Javier Segurado), fatma.karayagiz@cirp.de (Fatma Karayagiz), santos@cirp.de (Ubiratan Freitas), L.Noels@ulg.ac.be (Ludovic Noels)

mechanism in [15], and it has been shown that this model can capture the complex behavior of polymers, including the asymmetry between tension and compression by considering pressure dependency effects in the yield surface. Besides, as it will be shown here, when considering different characteristic visco-elastic times for the bulk and shear moduli, the Poisson's ratio is not constant but a function of time [16], allowing capurting different visco-elastic behaviors in tension and compression. Although the model parameters can be identified by following the hierarchical process described in [15], in which each experimental test response is used to identify a given parameter or parameters set, this deterministic identification process, conducted in [15] for a material process inducing less variability than additive manufacturing, remains manual and suffers from several limitations. On the one hand, uncertainties are unavoidably involved in the mechanical behaviors of laser sintered PA12. These uncertainties are not only due from the nontraditional fabrication process, but are also resulting from the experimental errors, since different machines are used to test the mechanical behavior under various loading directions and rates. A manual identification process, would thus require the user to make some assumptions on the curves to be considered for the identification, e.g. an "average" response curve, but the information related to the uncertainties would be lost. On the other hand the model is not necessarily rich enough to capture all the possible loading cases with a high accuracy. Proceeding with a manual deterministic hierarchical identification implies making choice on the test selected for the evaluation of a given parameter or parameters set, and there is no guarantee that the identified values would provide fair predictions for other loading tests. It is thus not straightforward to identify, using traditional optimization techniques, a set of material parameters which is a good compromise in terms of errors with respect to the different measurement data.

In order to circumvent the limitations of traditional deterministic optimization techniques, in this work, Bayesian Inference (BI) is applied to identify the constitutive parameters of the finite-strain VE-VP model [15] for laser sintered PA12. Bayesian Inference (BI) [17, 18] is a statistical method that allows updating ones's belief about a system or process based on new evidences or observations: in the BI approach, a prior probability distribution is assigned to the material parameters based on existing knowledge or assumptions, and this distribution is updated based on experimental data using Bayes' theorem. BI has been increasingly used in the field of material science for the identification of material properties: elasto-perfectly plastic model and cohesive zone parameters were inferred in [19], elasto-plastic material model parameters in [20–22], visco-elasticity constants in [23, 24] and a hyperelastic model and its parameters in [25], the list being non-exhaustive, we refer to the recent review of [26]. BI can also be used to infer multi-scale model parameters using observations at a higher scale [27–31] or spatially varying elasticity constants [32, 33]. Overall, BI provides a powerful framework for material properties identification that can improve the accuracy and reliability of material design and optimization.

One of the challenges in using BI for material properties identification is the selection of appropriate prior distributions. These prior distributions should reflect the existing knowledge and uncertainties about

the material parameters, while not being overly restrictive or informative. Another challenge is the computational cost of BI, especially when dealing with high-dimensional parameter spaces and complex models. Although advances in computational methods and the application of Gaussian process [26–28], kernel support vector machine model [34], Polynomial Chaos Expansion [31], or Neural Network (NNW) [22, 30] have made BI more accessible and practical for material properties identification, dealing with a complex material model remains a cumbersome task. On the one hand, massive material parameters are required to describe the complex behavior. On the other hand, massive experimental data are required to reveal those behaviors. Hence, the likelihood function would yield really low values, and it is difficult to reach convergence when using Markov Chain Monte Carlo (MCMC) random walk to generate samples in high-dimensional parameter spaces.

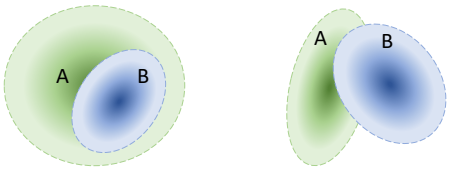

(a) (b)

Figure 1: Inferred material parameter ranges for experimental observations A and B, while (a) the parameter range for B is included in that of A, (b) the two ranges have partial overlap.

In this work, the finite-strain VE-VP formulation developed in [15] is adopted as the constitutive model for PA12 processed by SLS and a BI is carried out to identify the material properties for two different printing directions which are defined by "V"–vertical printing direction and "H"–horizontal printing direction. In order to capture the behavior reported by the available experimental data obtained for different loading cases, such as tension and compression, at different strain rates ranging from $10^{-4}\,\mathrm{s}^{-1}$ to $10^{3}\,\mathrm{s}^{-1}$, we have a total of 32 material parameters to be inferred. The pointed difficulties when dealing with this large amount of parameters are addressed by introducing the following ingredients:

- In order to reduce the arbitrary choice of visco-elastic and hardening material parameters, the number of visco-elastic branches and hardening laws terms are set as hyper-parameters which are determined according to the available experimental data, with the final sets of material parameters obtained from the BI.
- The challenge of the selection of appropriate prior distributions of the BI is overcome by using a sequential Bayesian Inference (SBI) process, in which part of the observations are used at a time. Wide prior distribution ranges of material parameters are first applied to avoid being overly restrictive or informative while these ranges are reduced gradually in the course of the sequential process.
- In order to avoid dealing with low likelihood values, the SBI not only involves part of the experimental

observations, but also subsets of the material parameters to be identified at a time, e.g. the visco-elastic parameters are first inferred before inferring the whole set of material parameters since the visco-plastic parameters do not affect the visco-elastic response. The convergence of MCMC random walk is hence improved.

- Various experimental data, such as tension, compression and relaxation, are used in the BI process. The feasible material parameter ranges for the different experimental observations could be included in one-another, see Fig. 1(a), or have partial overlap, see Fig. 1(b). The second case indicates a competition mechanism between material parameters. It means that a set of parameters that makes the model to perfectly fit one group of experimental observations can yield less good or even unacceptable fit for another group of observations. Because of the asymmetry between tension and compression in both the visco-elastic and visco-plastic parts, this competition appears when considering the tension and compression experimental observations in the identification of the pressure related parameters. Since we have much more experiments in compression than in tension, this would lead to inaccurate parameter sets for tensile tests if we treat all the experimental data equally since the weight of the tension data in the likelihood function would be much lower than that of the compression data. This issue is resolved by introducing a tension experimental observations augmentation in this work.

The results of MCMC random walk during the BI provide the distribution of material properties under the form of random vector realizations of massive data. Although the maximum a-posteriori (MAP) estimates of material properties could be extracted, this would correspond to loosing the information related to the uncertainties due to the measurement errors, the identification process and the model limitations[1], which need to be accounted for during mechanical analyses of structures. Therefore it would not be proper to use only the maximum a-posteriori (MAP) estimates of material properties in further numerical analyses. The advantage of BI is that it not only provides a reliable material parameter identification methodology, but it also preserves the inherent uncertainties of those parameters. The samples obtained from MCMC random walk provide a non-parametric representation of a high dimensional joint distribution of the random parameters. Instead of drawing parameter points from the massive samples directly following a uniform distribution of integer in range of 1 to the number of total samples, since each sample has equal probability, the random parameter points can be drawn according to their joint distributions. A generator serves as a nonlinear function which projects independent standard normal distributions to complex joint distributions. The main advantage of this latter approach is the ability to generate on demand an arbitrary number of realizations of the parameter samples, instead of repeating samples of the MCMC random walk. Therefore, based on the random vector realizations presented under the form of massive data by the MCMC random

[1] inherent material variations are not captured with a single BI see the discussion in [29]

walk, a random material parameter generator is constructed. This could be achieved using the diffusion map [35] as done in [36], but instead, in this work, a particular Neural Network (NNW) framework, a Generative Adversarial Network (GAN), is trained using the data obtained from MCMC random walk. In particular for PA12 printed along the "H" direction, whose random material properties show a bi-modal distribution, the random material properties are generated by combining a Bernoulli distribution with GANs. A good agreement is obtained between the distributions of the training data and the generated random material parameters. These generators can thus serve to create a synthetic data-set of the material parameters for the future structure analyses.

The organization of this paper is as follows. In Section 2, the manufacturing and testing protocol of the PA12 samples are reported. The VE-VP model able to capture the asymmetry between tension and compression by considering pressure dependency effects in both the visco-elastic and visco-plastic parts is summarized in Section 3. The SBI process with tension observations augmentation is presented in Section 4 and the results are illustrated in Section 5. The material parameters generator based on a GAN is developed in Section 6.

2. Preparation and mechanical experiments of PA12 samples

2.1. Selective Laser Sintering (SLS) PA12 samples manufacturing process

The SLS 3D printer Formiga P100 and the white polyamide powder PA2200 from Electro-Optical Systems GmbH (EOS) are used to print the testing samples. The manufacturing process follows 3 steps: i) Pre-process; ii) Printing Process; and iii) Post process.

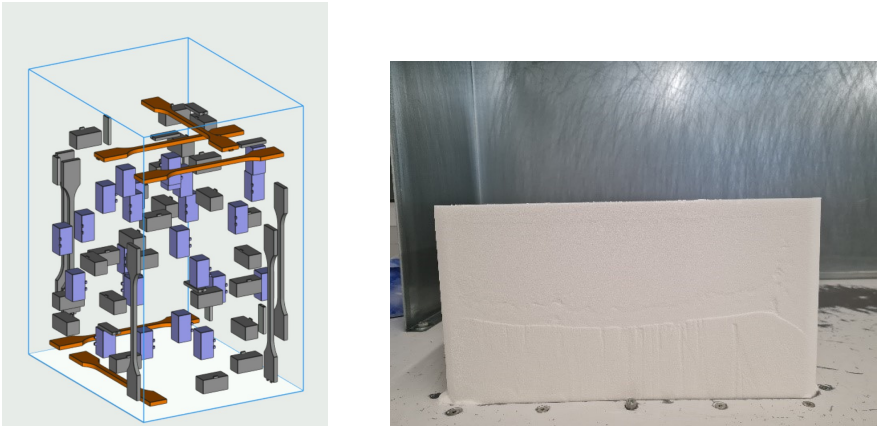

(a) (b)

Figure 2: SLS printing: (a) Building job side view with the "H" specimens in violet and gray for respectively compression and tensile, and the "V" specimens in gray and orange for respectively compression and tensile; and (b) Powder cake (Source: cirp GmbH).

In the pre-process, 50% new and 50% old PA2200 powder is mixed and sieved. Before printing, the machine is first cleaned, and then a 6 mm bottom layer of powder is applied to ensure homogeneous building temperature and prevent deviations. The machine is pre-heated during 2h with the temperature of 169°C (chamber temperature) on the building area and 150°C for removal chamber temperature. After pre-heating and before the first components are printed, an additional 9 mm layer of powder is applied. This layer serves as a thermal isolation.

The geometries of the parts to be printed are distributed in the build volume of the printer. All components are packed freely in the installation space in such a way that the total height is kept as low as possible and the individual layers are as uniform as possible in order to keep the energy curve and individual layer duration as uniform as possible. Finally, the samples were built with a packing density of 5.86% distributed over the overall height of 268.22 mm, see Fig. 2(a), in which the non-relevant components have been hidden. The resolution of the components results from the layer thickness of 0.1 mm and laser focus diameter 0.5 mm.

After printing, the build volume is slowly cooled down inside the printer. This cool down time is chosen at least as long as of the printing duration. Both printing and cooling in the machine take place under a nitrogen atmosphere. With the help of the slow cooling, effects such as warpage are reduced. After printing and cooling, the printed parts and the non-sintered powder form a block called powder "cake". The cake is then removed from the system as shown in Fig. 2(b). In the post-treatment, the components are removed from the powder cake after cooling, roughly de-powdered and then sandblasted to remove the remaining powder from the surface.

2.2. Experiments conducted on the PA12 samples

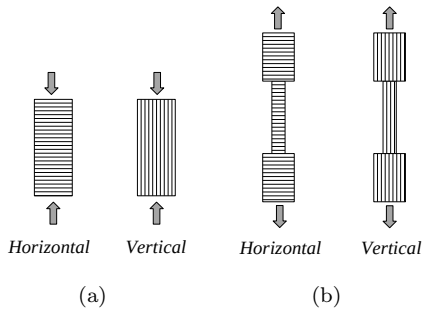

Figure 3: PA12 test samples: (a) Compression test specimens; and (b) Tensile test specimens.

All the samples were built using the same machine and parameters within a single batch to exclude variability between sets. Specimens are characterized at two different building directions, where the specimens are printed with layers perpendicular or parallel to the loading direction, denoted as "H" and "V", respectively, see Fig. 3. In Fig. 2(a), the "H" Specimens are the violet and gray ones for respectively

compression and tensile, and the "V" Specimens are the gray and orange ones for respectively compression and tensile. Uniaxial tensile, compression and relaxation tests were performed on samples of PA12 on both building directions.

2.2.1. Uniaxial Tensile Tests

Dogbone-shaped specimens printed along both directions with standardized ASTM D360 dimensions of initial length $L_0 = 113$ mm, width $W_0 = 5$ mm, and thickness $T_0 = 4.1$ mm were used for tensile testing. Tests were performed using an *INSTRON 5966* with a load cell of 2 kN at 7.37×10^{-4}, 7.37×10^{-3} and 7.37×10^{-2} s^{-1} strain rates. The tests were performed following the ASTM D360 standard.

2.2.2. Uniaxial Compression Tests

Uniaxial compression tests were performed on PA12 specimens printed along both directions at a wide range of strains. For low strain rates (2.78×10^{-3}, 2.78×10^{-2} and 2.78×10^{-1} s^{-1}), tests were done on an *INSTRON 3384* universal testing machine, for medium (1 and 10 s^{-1}), tests were performed on a *Gleeble 3800 GTC*, and for high strain rates (160 to 890 s^{-1}), *Split-Hopkinson pressure bar* was used. For low strain rates, flat specimens of standard dimensions of initial length $L_0 = 30$ mm, and a square cross section of 15 mm per side were used, and for medium and high strain rates, cylindrical specimens of 18 mm height and a diameter of 12 mm were used.

2.2.3. Stress Relaxation Tests of PA12

To study the visco-elastic-visco-plastic behavior of PA12, uniaxial stress relaxation tests were performed on samples along both building directions. Two different maximum strains and a holding period of 30 minutes were chosen to study the relaxation in the elastic and plastic regimes. A set of specimens were compressed to a maximum strain of 0.02 and others of 0.3 at (2.78×10^{-3} s^{-1}). The samples dimensions and machine used are identical to the ones used in compression tests at low strain rates.

The measured stress-strain curves for compression and tensile tests, and stress-time curves for relaxation tests will be presented in Section 4.2. More details about the experiments can be found in [10].

3. Hyperelastic visco-elastic-visco-plastic material model

Experimental result shows that SLS-printed PA12 presents visco-elasto-visco-plastic behavior with moderate strain rate sensitivity on the yield stress and an asymmetry between tension and compression both in the visco-elastic and visco-plastic parts. The response of this polyamide material can be represented using a finite-strain visco-elastic visco-plastic material models with a pressure dependency effect. The hyperelastic visco-elastic-visco-plastic material model presented in [15] is adopted in this work and the damage related

mechanism introduced in [15] is omitted. The basic equations of the constitutive law are summarized for the case of isotropic plastic hardening and the required material parameters are clarified in this section.

In the current configuration, the position $\mathbf{x}$ of a material point is a function of time t and its position $\mathbf{X}$ in the reference configuration. The deformation state is described by the deformation gradient which reads

$$\mathbf{F} = \frac{\partial \mathbf{x}}{\partial \mathbf{X}}\,, \tag{1}$$

with its Jacobian $J = \det\mathbf{F} > 0$. For visco-elastic-visco-plastic material, the deformation gradient is decomposed into visco-elastic and visco-plastic parts, following multiplicative decomposition [37], which yields

$$\mathbf{F} = \mathbf{F}^{\mathrm{ve}} \cdot \mathbf{F}^{\mathrm{vp}}\,. \tag{2}$$

The so-called visco-plastic strain rate tensor $\mathbf{D}^{\mathrm{vp}}$ is defined as the symmetric part of the visco-plastic spatial gradient of velocity $\mathbf{L}^{\mathrm{vp}}$, which reads

$$\mathbf{L}^{\mathrm{vp}} = \dot{\mathbf{F}}^{\mathrm{vp}} \cdot \mathbf{F}^{\mathrm{vp}\,-1}\,. \tag{3}$$

By assuming a symmetric $\mathbf{L}^{\mathrm{vp}}$, it yields

$$\mathbf{D}^{\mathrm{vp}} = \mathbf{L}^{\mathrm{vp}}\,, \text{ and } \dot{\mathbf{F}}^{\mathrm{vp}} = \mathbf{D}^{\mathrm{vp}} \cdot \mathbf{F}^{\mathrm{vp}}\,. \tag{4}$$

The evolution of $\mathbf{D}^{\mathrm{vp}}$ is governed by the visco-plastic flow rule, further described.

3.1. Strain and stress in visco-elastic part

The visco-elastic behavior is modeled by the generalized Maxwell model with one spring and N Maxwell elements in parallel. The logarithmic strain measure is adopted in [15] and defined as

$$\mathbf{E} = \frac{1}{2}\ln\mathbf{C}\,, \text{ and } \mathbf{E}^{\mathrm{ve}} = \frac{1}{2}\ln\mathbf{C}^{\mathrm{ve}}\,, \tag{5}$$

with the right Cauchy strain tensor $\mathbf{C} = \mathbf{F}^{\mathrm{T}} \cdot \mathbf{F}$, and $\mathbf{C}^{\mathrm{ve}} = \mathbf{F}^{\mathrm{veT}} \cdot \mathbf{F}^{\mathrm{ve}}$. Its conjugated visco-elastic stress measure $\boldsymbol{\tau}$ is interpreted as a corotational Kirchhoff stress and can be derived from a logarithmic elastic potential and a quadratic dissipating function [13], or directly expressed in terms of the visco-elastic functions as

$$\operatorname{dev}\boldsymbol{\tau}(t) = \int_{-\infty}^{t} 2G(t-s)\frac{\mathrm{d}}{\mathrm{d}s}\operatorname{dev}\mathbf{E}^{\mathrm{ve}}(s)\mathrm{d}s\,, \tag{6}$$

$$p = \frac{1}{3}\mathrm{tr}\boldsymbol{\tau} = \int_{-\infty}^{t} K(t-s)\frac{\mathrm{d}}{\mathrm{d}s}\mathrm{tr}\,\mathbf{E}^{\mathrm{ve}}(s)\mathrm{d}s\,, \tag{7}$$

where the time functions of shear and bulk moduli are given by the Maxwell model and read

$$G(t) = G_\infty + \sum_{i=1}^{N} G_i e^{-t/g_i}\,, \tag{8}$$

$$K(t) = K_\infty + \sum_{i=1}^{N} K_i e^{-t/k_i}\,. \tag{9}$$

Then, the stress $\boldsymbol{\tau}$ is estimated from its deviatoric and volumetric parts by

$$\boldsymbol{\tau} = \operatorname{dev} \boldsymbol{\tau} + p\mathbf{I}\,, \tag{10}$$

with the first Piola-Kirchhoff stress $\mathbf{P}$ arising from

$$\mathbf{P} = (\mathbf{F}^{\mathrm{ve}})^{\text{-T}} \cdot \boldsymbol{\tau} \cdot (\mathbf{F}^{\mathrm{vp}})^{\text{-T}}\,. \tag{11}$$

In this visco-elastic stage, the material parameters that need to be identified are

- the shear moduli G_∞, G_i $(i = 1, ..., N)$,
- the bulk moduli K_∞, K_i $(i = 1, ..., N)$, and
- their corresponding characteristic relaxation times g_i, k_i $(i = 1, ..., N)$, see Eqs. (8) and (9),

where N is a hyper-parameter that needs to be chosen before conducting the parameter identification. We note that the asymmetry between tension and compression in the visco-elastic response can be captured by considering different characteristic relaxation times g_i, k_i for the shear and bulk moduli.

3.2. Visco-Plastic part

The visco-elastic region is limited by a pressure-sensitive yield condition. The non-associated Perzyna-type visco-plastic flow rule [14] is used for the studied material and reads

$$\mathbf{D}^{\mathrm{vp}} = \frac{1}{\eta} \langle f \rangle^{\frac{1}{s}} \mathbf{Q} = \lambda \mathbf{Q}\,, \tag{12}$$

where f is the yield function, $\langle \bullet \rangle$ denotes the Macauley brackets defined by $\langle f \rangle = \frac{1}{2}(f + |f|)$, η and s are respectively the viscosity and rate sensitivity parameters, and where $\mathbf{Q} = \frac{\partial P}{\partial \boldsymbol{\tau}}$ is the normal to the plastic flow potential P. The visco-plastic consistency parameter $\lambda = \frac{1}{\eta} \langle f \rangle^{\frac{1}{s}}$ leads to a reformulation of the yield function which reads

$$\bar{f} = f - (\eta\lambda)^s \leq 0\,, \tag{13}$$

and is subject to the Kuhn-Tucker condition,

$$\lambda \bar{f} = 0\,, \lambda \geq 0 \text{ and } \bar{f} \leq 0\,. \tag{14}$$

3.2.1. Yield function f

The pressure-dependent yield function f is expressed in terms of the corotational Kirchhoff stress $\boldsymbol{\tau}$, considering isotropic hardening only, as

$$f(\boldsymbol{\tau}) = a_2 \tau_{\mathrm{e}}^{\alpha} - a_1 p - a_0\,, \tag{15}$$

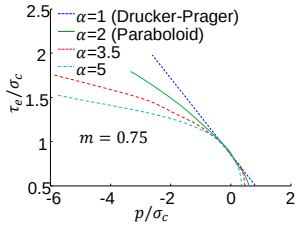

Figure 4: Effect of the material parameter α on the yield function (15).

where the pressure term p is given in Eq. (7), $\tau_{\mathrm{e}} = \sqrt{\frac{3}{2}\mathrm{dev}\boldsymbol{\tau} : \mathrm{dev}\boldsymbol{\tau}}$ is the equivalent stress, and the material parameter α enhances the Drucker-Prager pressure-dependency description. As illustrated in Fig. 4, this parameter α allows capturing more complex pressure effects on the yield function, compared to the linear Drucker-Prager model, which has been shown to overestimate the yield function for negative pressure in the case of polymeric materials as discussed in [15]. The coefficients a_0, a_1 and a_2 are functions of the equivalent plastic strain and are introduced in order to model the isotropic hardening of the yield surface.

Under uniaxial compressive and tensile loading conditions, at the onset of plastic flow, we have respectively,

$$\begin{cases} a_2(\sigma_{\mathrm{c}})^{\alpha} - a_1 \frac{-\sigma_{\mathrm{c}}}{3} - a_0 = 0 \\ a_2(\sigma_{\mathrm{t}})^{\alpha} - a_1 \frac{\sigma_{\mathrm{t}}}{3} - a_0 = 0 \end{cases} \tag{16}$$

where σ_{c} and σ_{t} are the current compressive and tensile, respectively, yield stress absolute values. Hence, using Eq. (16), the coefficients a_0, a_1 and a_2 can be expressed in terms of the these current yield stresses as

$$\begin{cases} a_1 = 3\frac{(\sigma_{\mathrm{t}})^{\alpha} - (\sigma_{\mathrm{c}})^{\alpha}}{\sigma_{\mathrm{t}} + \sigma_{\mathrm{c}}} a_2 \,, \\ a_0 = \frac{(\sigma_{\mathrm{t}})^{\alpha}\sigma_{\mathrm{c}} + (\sigma_{\mathrm{c}})^{\alpha}\sigma_{\mathrm{t}}}{\sigma_{\mathrm{t}} + \sigma_{\mathrm{c}}} a_2 \,, \end{cases} \tag{17}$$

where a_2 can be an arbitrary non-zero value, and is chosen to be $a_2 = \frac{1}{(\sigma_{\mathrm{c}})^{\alpha}}$. By defining a tension-compression flow asymmetry parameter $m = \frac{\sigma_{\mathrm{t}}}{\sigma_{\mathrm{c}}}$, Eqs. (17) result into

$$a_2 = \frac{1}{(\sigma_{\mathrm{c}})^{\alpha}},\ a_1 = 3\frac{m^{\alpha} - 1}{m + 1}\frac{1}{\sigma_{\mathrm{c}}} \text{ and } a_0 = \frac{m^{\alpha} + m}{m + 1}\,, \tag{18}$$

in which the current yield stresses σ_{t} and σ_{c} are defined as functions of the equivalent plastic strain γ to model the effect of plastic hardening.

3.2.2. Flow potential P

A quadratic function is used as the plastic flow potential in [15], which reads,

$$P = \tau_{\mathrm{e}}^2 + \beta p^2\,, \tag{19}$$

where τ_{e} and p are the pressure and equivalent stress, and β is a material parameter governing the volumetric plastic deformation, e.g. $\beta = 0$ indicates a zero volumetric plastic deformation.

3.2.3. The equivalent plastic strain γ and plastic hardening

The equivalent plastic strain γ is defined from the plastic strain rate tensor as

$$\dot{\gamma} = k\sqrt{\mathbf{D}^{\mathrm{vp}} : \mathbf{D}^{\mathrm{vp}}}\,, \tag{20}$$

where

$$k = \frac{1}{\sqrt{1+2\nu_{\mathrm{p}}^2}}\,, \tag{21}$$

with ν_{p} being the plastic Poisson's ratio. This plastic Poisson's ratio is assumed to be constant and is related to β at the plastic flow onset [38] by

$$\nu_{\mathrm{p}} = \frac{9-2\beta}{18+2\beta}\,. \tag{22}$$

The isotropic hardening functions define distinctive tensile and compressive yield stress evolutions, which are modeled independently by

$$\dot{\sigma_{\mathrm{t}}} = H_{\mathrm{t}}(\gamma)\dot{\gamma}\,,\ \text{with}\ \sigma_{\mathrm{t}}(\gamma=0) = \sigma_{\mathrm{t}}^0\,,\ \text{and} \tag{23}$$

$$\dot{\sigma_{\mathrm{c}}} = H_{\mathrm{c}}(\gamma)\dot{\gamma}\,,\ \text{with}\ \sigma_{\mathrm{c}}(\gamma=0) = \sigma_{\mathrm{c}}^0\,, \tag{24}$$

where σ_{t}^0 and σ_{c}^0 are respectively the initial tensile and compressive yield stresses. The isotropic hardening functions $H_{\mathrm{t}}(\gamma)$ and $H_{\mathrm{c}}(\gamma)$ follow the general forms,

$$H_{\mathrm{t}}(\gamma) = \sum_{i=0}^{M_{\mathrm{t}}} t_i\gamma^i + h_{\mathrm{t}}H_{\mathrm{t}}^0 e^{-h_{\mathrm{t}}\gamma}\,, \tag{25}$$

$$H_{\mathrm{c}}(\gamma) = \sum_{i=0}^{M_{\mathrm{c}}} c_i\gamma^i + h_{\mathrm{c}}H_{\mathrm{c}}^0 e^{-h_{\mathrm{c}}\gamma}\,, \tag{26}$$

where M_{t} and M_{c} are the polynomial orders, and t_i $(i=0,...,M_{\mathrm{t}})$, c_i $(i=0,...,M_{\mathrm{c}})$, H_{t}^0, H_{c}^0, h_{t} and h_{c} are the material parameters of the plastic hardening laws.

In this visco-plastic stage with isotropic hardening, the required material parameters are

- visco-plastic parameters: η and s in Eq. (12);
- yield function: α in Eq. (18), initial tensile and compressive yield stresses σ_{t}^0 and σ_{c}^0;
- flow potential parameter: β in Eq. (19);
- hardening parameters: t_i $(i=0,...,M_{\mathrm{t}})$, c_i $(i=0,...,M_{\mathrm{c}})$, H_{t}^0, H_{c}^0, h_{t} and h_{c} in Eqs. (25) and (26), where M_{t} and M_{c} are the hyper-parameters that need to be chosen before performing the parameter identification.

The detailed implementation and resolution of the material model can be found in [15], and is omitted here.

4. SLS-printed PA12 parameter identification with Sequential Bayesian inference (SBI)

4.1. Bayesian Inference (BI) theory

Based on the Bayes' theorem, the statistical analysis approach called Bayesian Inference (BI) states that the posterior probability of a random parameters vector $\boldsymbol{\alpha} \in \mathbb{R}^n$ for given observation events, such as the realizations of a random vector $\boldsymbol{\beta} \in \mathbb{R}^m$, $\pi(\boldsymbol{\alpha}|\boldsymbol{\beta})$, is proportional to the prior probability $\pi(\boldsymbol{\alpha})$ multiplied by the likelihood of $\boldsymbol{\beta}$ with given observations of $\boldsymbol{\alpha}$:

$$\pi(\boldsymbol{\alpha}|\boldsymbol{\beta}) = \frac{\pi(\boldsymbol{\alpha})\pi(\boldsymbol{\beta}|\boldsymbol{\alpha})}{\pi(\boldsymbol{\beta})}\,, \tag{27}$$

where $\pi(\bullet)$ ($\pi(\bullet|\bullet)$) denotes a (conditional) Probability Density Function (PDF).

Since $\pi(\boldsymbol{\beta})$ is a constant for given observations, BI is often written as

$$\pi_{\text{post}}(\boldsymbol{\alpha}|\boldsymbol{\beta}) \propto \pi(\boldsymbol{\beta}|\boldsymbol{\alpha})\pi_{\text{prior}}(\boldsymbol{\alpha})\,, \tag{28}$$

where the subscripts "prior" refers to the prior distribution $\pi(\boldsymbol{\alpha})$ which reflects the initial belief or knowledge one has on $\boldsymbol{\alpha}$, "post" refers to the posterior distribution of the random vector $\boldsymbol{\alpha}$ that accounts for the observation data $\boldsymbol{\beta}$, and where the conditional PDF $\pi(\boldsymbol{\beta}|\boldsymbol{\alpha})$, which is constructed from the different observation data $\boldsymbol{\beta}$, is called the likelihood function.

4.1.1. Sequential Bayesian inference

In theory, Bayesian inference is able to identify the whole set of material parameters all together. However, in practice, the model can be defined by an important number of parameters that need to be identified for a given physical process, while a lot of observation data should be involved to conduct the inference. When using all the experimental observation data at once leads to low values of likelihood function. As a consequence, for a high number of parameters to be identified the convergence of random walk in BI becomes too slow to be conducted. In particular, when the prior distribution ranges of the parameters are wide and a lot of extra computations are needed, it could be difficult to carry out the BI within a reasonable time. But since the posterior can act as the prior of a new BI if additional data are observed subsequently, and using the initial knowledge on the material model –the visco-plastic properties have no effects on the visco-elastic response of the material at small deformation– the Bayesian inference can be performed sequentially. The sequential BI in which the priors of some parameters arise from the posterior of a previous inference process, involves reduced observation data, less wide prior distributions for part of the parameters and thus alleviates the previously listed difficulties.

In the sequential BI, the random parameters and observations sets are both divided into two parts: $\boldsymbol{\alpha} = [\boldsymbol{\alpha}_1, \boldsymbol{\alpha}_2]$ and $\boldsymbol{\beta} = [\boldsymbol{\beta}_1, \boldsymbol{\beta}_2]$, e.g. $\boldsymbol{\alpha}_1$ and $\boldsymbol{\beta}_1$ can be the parameters and observations associated to the

elastic behavior, while $\boldsymbol{\alpha}_2$ and $\boldsymbol{\beta}_2$ would be the ones associated to the plastic response. The Eq. (28) then becomes

$$\pi_{\text{post}}\left(\boldsymbol{\alpha}_1,\, \boldsymbol{\alpha}_2|\boldsymbol{\beta}_1,\, \boldsymbol{\beta}_2\right) \propto \pi\left(\boldsymbol{\beta}_1,\, \boldsymbol{\beta}_2|\boldsymbol{\alpha}_1,\, \boldsymbol{\alpha}_2\right) \pi_{\text{prior}}\left(\boldsymbol{\alpha}_1,\, \boldsymbol{\alpha}_2\right) . \tag{29}$$

The random parameters can be assumed to be independent in the prior stage, hence

$$\pi_{\text{prior}}\left(\boldsymbol{\alpha}_1,\, \boldsymbol{\alpha}_2\right) = \pi_{\text{prior}}\left(\boldsymbol{\alpha}_1\right) \pi_{\text{prior}}\left(\boldsymbol{\alpha}_2\right) , \tag{30}$$

and the observations $\boldsymbol{\beta}_1$ and $\boldsymbol{\beta}_2$ are conditionally independent, which gives

$$\pi\left(\boldsymbol{\beta}_1,\, \boldsymbol{\beta}_2|\boldsymbol{\alpha}_1,\, \boldsymbol{\alpha}_2\right) = \pi\left(\boldsymbol{\beta}_2|\,\boldsymbol{\alpha}_1,\, \boldsymbol{\alpha}_2\right) \pi\left(\boldsymbol{\beta}_1|\boldsymbol{\alpha}_1,\, \boldsymbol{\alpha}_2\right) . \tag{31}$$

Then using Eqs. (30) and (31), Eq. (29) is rewritten as

$$\pi_{\text{post}}\left(\boldsymbol{\alpha}_1,\, \boldsymbol{\alpha}_2|\boldsymbol{\beta}_1,\, \boldsymbol{\beta}_2\right) \propto \pi(\boldsymbol{\beta}_2|\,\boldsymbol{\alpha}_1,\, \boldsymbol{\alpha}_2)\pi_{\text{prior}}\left(\boldsymbol{\alpha}_2\right) \underline{\pi\left(\boldsymbol{\beta}_1|\boldsymbol{\alpha}_1,\, \boldsymbol{\alpha}_2\right) \pi_{\text{prior}}\left(\boldsymbol{\alpha}_1\right)} . \tag{32}$$

If it is initially known that the parameters $\boldsymbol{\alpha}_2$ will have no effects on the random vectors corresponding to the observations $\boldsymbol{\beta}_1$, e.g. the visco-plastic properties have no effects on the visco-elastic response of the material at small deformation observations, the underlined term in Eq. (32) is simplified to $\pi(\boldsymbol{\beta}_1|\boldsymbol{\alpha}_1)\pi_{\text{prior}}(\boldsymbol{\alpha}_1)$. According to Eq. (28), we have

$$\pi_{\text{post}}(\boldsymbol{\alpha}_1|\boldsymbol{\beta}_1) \propto \pi(\boldsymbol{\beta}_1|\boldsymbol{\alpha}_1)\pi_{\text{prior}}(\boldsymbol{\alpha}_1) , \tag{33}$$

and then Eq. (32) yields

$$\pi_{\text{post}}\left(\boldsymbol{\alpha}_1,\, \boldsymbol{\alpha}_2|\boldsymbol{\beta}_1,\, \boldsymbol{\beta}_2\right) \propto \pi\left(\boldsymbol{\beta}_2|\,\boldsymbol{\alpha}_1,\, \boldsymbol{\alpha}_2\right) \pi_{\text{prior}}\left(\boldsymbol{\alpha}_2\right) \pi_{\text{post}}\left(\boldsymbol{\alpha}_1|\boldsymbol{\beta}_1\right) . \tag{34}$$

The expressions in Eqs. (33) and (34) can be stated as a sequence of BI in which the parameters $\boldsymbol{\alpha}_1$ are inferred using observation data $\boldsymbol{\beta}_1$ first to define a new prior distribution of $\boldsymbol{\alpha}_1$ under the form of the obtained posterior distribution $\pi_{\text{post}}\left(\boldsymbol{\alpha}_1|\boldsymbol{\beta}_1\right)$. This new prior distribution is then used when conducting the BI of $\boldsymbol{\alpha} = [\boldsymbol{\alpha}_1,\, \boldsymbol{\alpha}_2]$, yielding the final posterior $\pi_{\text{post}}\left(\boldsymbol{\alpha}_1,\, \boldsymbol{\alpha}_2|\boldsymbol{\beta}_1,\, \boldsymbol{\beta}_2\right)$. It can be seen that only a part of the observation data is used in each likelihood function in Eqs. (33) and (34), and either the number of identified parameters is reduced or the prior distribution ranges are reduced in each step of the sequential BI.

4.1.2. Error-based inference and likelihood function

An error-based BI is considered in the present work. In this context, the adopted constitutive model is expressed in a simple form for the case of uniaxial monotonic loading as

$$\sigma_{\text{eng}}(\varepsilon,\, \dot{\varepsilon},\, t;\, \boldsymbol{\vartheta}) = \Phi(\varepsilon,\, \dot{\varepsilon},\, t;\, \boldsymbol{\vartheta}) , \tag{35}$$

where $\boldsymbol{\vartheta}$ represents the material parameters to be inferred, the engineering stress σ_{eng} is extracted from the first Piola-Kirchhoff stress with $\sigma_{\text{eng}} = P_{11}$, the engineering strain ε relates to the deformation gradient through $\varepsilon = F_{11} - 1$, $\dot{\varepsilon}$ is the time rate of ε, and where the loading time t is used in the case of relaxation test, otherwise t can be replaced by $\varepsilon/\dot{\varepsilon}$. The relation between a stress measurement Σ and the model response is written as

$$\Sigma = \sigma_{\text{eng}} + \omega_\Sigma = \Phi(\varepsilon,\, \dot{\varepsilon},\, t;\, \boldsymbol{\vartheta}) + \omega_\Sigma \,, \tag{36}$$

where the stress noise ω_Σ follows a Gaussian distribution $\mathcal{N}(x|0,\, s_\Sigma^2)$ of standard deviation s_Σ with

$$\mathcal{N}\left(x|0,\, s_\Sigma^2\right) = \frac{1}{s_\Sigma\sqrt{2\pi}} \exp\left[-\frac{1}{2}\left(\frac{x}{s_\Sigma}\right)^2\right]. \tag{37}$$

Therefore, the conditional distribution of measured stress reads

$$\pi\left(\Sigma|\varepsilon,\, \dot{\varepsilon},\, t,\, \boldsymbol{\vartheta}\right) = \mathcal{N}\left(\Sigma - \Phi\left(\varepsilon,\, \dot{\varepsilon},\, t;\, \boldsymbol{\vartheta}\right)|0,\, s_\Sigma^2\right) \,. \tag{38}$$

We now consider N_β observations extracted from different experimental samples, each sample being tested for a given loading case such as compression, tension or relaxation, with several observations taken for each tested samples, N_β being the total number of gathered observations for the different loading cases. Assuming that each experimental test is independent from the other ones and using the theory of conditional independence [39], the likelihood function reads[2]

$$\pi\left(\boldsymbol{\Sigma}|\boldsymbol{\varepsilon},\, \dot{\boldsymbol{\varepsilon}},\, \boldsymbol{t},\, \boldsymbol{\vartheta}\right) = \prod_{i=1}^{N_\beta} \mathcal{N}\left(\Sigma_i - \Phi\left(\varepsilon_i,\, \dot{\varepsilon}_i,\, t_i;\, \boldsymbol{\vartheta}\right)|0,\, s_{\Sigma_i}^2\right) \,, \tag{39}$$

where $\boldsymbol{\varepsilon} = \left[\varepsilon_1, ..., \varepsilon_{N_\beta}\right]$ and $\boldsymbol{t} = \left[t_1, ..., t_{N_\beta}\right]$ are respectively the vectors of observation strains and times defined in Eq. (35), and where $\boldsymbol{\Sigma} = \left[\Sigma_1, ..., \Sigma_{N_\beta}\right]$, with Σ_i the stress observation corresponding to a given experiment type –compression, tension or relaxation, at ε_i, $\dot{\varepsilon}_i$ and t_i.

Normally, the standard deviations s_{Σ_i} are estimated from the repeated experimental measurements. However, in order to increase the robustness of the BI process, we assume

$$s_{\Sigma_i} = \varsigma\, \mathbb{E}\left(\Sigma_i\right) \,, \tag{40}$$

[2]For the N_d data points extracted from one experimental sample of a defined unique loading path, the measured stresses Σ_i at different strain levels ε_i are correlated: the correlation among the experimental measurements results from the unique material properties of a given tested sample. In all generality, the likelihood function is built, using the data points from one sample, as

$$\pi\left(\Sigma_1,\, ...,\, \Sigma_{N_d}|\varepsilon_1,\, ...,\, \varepsilon_{N_d},\, t_1,\, ...,t_{N_d},\, \boldsymbol{\vartheta}\right) \,.$$

Since the correlations among the measured stresses is assumed to result solely from the shared material properties, when these material properties are given, the probability distributions of the stresses become independent. Since strain ε_i has no effect on the stress Σ_j, $i \neq j$, using the theory of conditional independence, the likelihood function can be factorized into $\prod_{i=1}^{N_d} \pi\left(\Sigma_i|\varepsilon_i,\, t_i,\, \boldsymbol{\vartheta}\right)$. Now considering a total of N_β observations from several independent tests, with N_d observations per single test, leads to (39).

where ς is a random variable and follows a prior distribution $\pi_{\text{prior}}(\varsigma)$, and where $\mathbb{E}(\Sigma_i)$ is the expectation of Σ_i. Then, the likelihood function (39) can be rewritten as

$$\pi(\boldsymbol{\Sigma}|\boldsymbol{\varepsilon}, \dot{\boldsymbol{\varepsilon}}, \boldsymbol{t}, \boldsymbol{\vartheta}) = \int \prod_{i=1}^{N_\beta} \mathcal{N}\left(\Sigma_i - \Phi(\varepsilon_i, \dot{\varepsilon}_i, t_i, \boldsymbol{\vartheta}) | 0, s^2_{\Sigma_i}\right) \pi_{\text{prior}}(\varsigma) \, \mathrm{d}\varsigma \,, \tag{41}$$

where the likelihood function can be regarded as the conditional Gaussian multiplied by a prior variance distribution, which is defined through ς, and integrated to obtain a marginal distribution. Since it is a sum of infinite Gaussian and has a long "tail" in general, this gives the likelihood an important property called robustness, which means that it is much less sensitive than the Gaussian to the presence of a few data points which are outliers. In practice, although an extra random variable ς is involved, the likelihood function (39) is still used in the MCMC random walk, and the integration with respect to ς can be carried out after sampling in order to obtain the marginal distribution.

4.2. PA12 parameter inference

Table 1: Mechanical experimental test types and strain rates.

Loading speed	experiment type	Strain rate $\dot{\varepsilon}$ [s^{-1}]
Low	Tension	7.37×10^{-4}
		7.37×10^{-3}
		7.37×10^{-2}
	Compression	2.78×10^{-3}
		2.78×10^{-2}
		2.78×10^{-1}
Medium	Compression	1.0
		10.0
High	Compression	~ 160
		~ 380.0
		~ 640.0
		~ 750.0
		~ 890.0
Relaxation (compression)	Elastic loading	2.78×10^{-3}
	Elasto-plastic loading	2.78×10^{-3}

4.2.1. Hyper-parameters

Before starting the BI process, a few hyper-parameters of the hyperelastic visco-elastic-visco-plastic model need to be set. These hyper-parameters are the number of parallel Maxwell elements N in Eqs. (8) and (9), and isotropic plastic hardening polynomial orders M_{t} and M_{c} in Eqs. (25) and (26).

Although the time functions of shear and bulk moduli could have different number of parallel Maxwell elements, the same number N is used for both shear and bulk parts in this work. The uniaxial tension, compression and relaxation tests listed in table 1 were carried out on PA12 specimens, see Section 2. The number N is chosen based on the available experimental data and the following facts.

- The testing strain rates vary from 10^{-4}/s to 10^{3}/s, and the relaxation test lasts 1800 s.
- In the relaxation test, no obvious stress decrease has been seen after 1000 s.
- The visco-elastic parameters will be determined using the experimental data with the absolute strain below 0.02.

From these observations, we can say that the range of characteristic relaxation times, g_i and k_i $(i = 1, ..., N)$, which are to be identified, is from 10^{-5} s ($\propto \frac{0.02}{10^{3}\,\mathrm{s}^{-1}}$) to 10^{2} s. Although the "real" characteristic relaxation times could be out of this range, they cannot be identified with the available experiment data. Hence, $N = 8$ is chosen to have the characteristic relaxation times of orders $\propto 10^{-5}$, $\propto 10^{-4}$, $\propto 10^{-3}$, $\propto 10^{-2}$, $\propto 10^{-1}$, $\propto 10^{0}$, $\propto 10^{1}$ and $\propto 10^{2}$ s, covering the whole experimental range while remaining accurate.

Besides, the orders $M_{\mathrm{t}} = 0$ and $M_{\mathrm{c}} = 0$ will be used for the isotropic plastic hardening polynomial laws in Eqs. (25) and (26) in order to minimize the number of material parameters.

Finally,

$$N = 8\,, M_{\mathrm{t}} = 0, \text{ and } M_{\mathrm{c}} = 0\,, \tag{42}$$

are the chosen hyper-parameters of the adopted material model.

4.2.2. Material parameters to be inferred and their prior distributions

The material parameters have been introduced and clarified in Section 3. The random variables for material properties with the chosen hyper-parameters will be presented in this section. These random material parameters are noted as $\boldsymbol{\vartheta}$, and divided into two groups $\boldsymbol{\vartheta} = \{\boldsymbol{\vartheta}^{\mathrm{ve}}, \boldsymbol{\vartheta}^{\mathrm{vp}}\}$.

Visco-Elastic (VE) parameters $\boldsymbol{\vartheta}^{ve}$. For a general linear visco-elastic model, the time functions of shear and bulk moduli, Eqs. (8) and (9), can have the number of Maxwell elements increased without limit [16], and be expressed in a continuous form. Such form of for the shear modulus, e.g., reads

$$G(t) = G_\infty + \int_0^\infty F_G(g) e^{-t/g} \mathrm{d}g = G_\infty + \int_{-\infty}^\infty H_G(g) e^{-t/g} \mathrm{d}\ln g\,. \tag{43}$$

Therefore, there are various choices to substitute an integral, see Eq. (43), by a summation of limited terms, even in a predefined relaxation time range. In order to remove this arbitrariness, we chose two characteristic relaxation times, g_1 and k_1, as the random variables to be inferred, and let the rest of them satisfy $g_i = g_1 \times 10^{-(i-1)}$ and $k_i = k_1 \times 10^{-(i-1)}$ for $i = 2, ..., 8$.

Using uniaxial tests, it is straightforward to identify the parameters of time function for the Young's modulus, $E(t)$, with a constant Poisson's ratio, when isotropic constitutive is considered. However, the Poisson's ratio, ν, of polymer material is not constant but a function of time [16]. In order to take this effect into account, the bulk moduli K_i ($i = 1, ..., 8$) and shear moduli G_i ($i = 1, ..., 8$) are used as random variables to be inferred, respectively. As for the equilibrium moduli, the Young's modulus E_∞ is adopted together with the Poisson's ratio ν_∞, with

$$G_\infty = \frac{E_\infty}{2(1+\nu_\infty)} \text{ and } K_\infty = \frac{E_\infty}{3(1-2\nu_\infty)}\,. \tag{44}$$

Independent uniform distributions will be used to construct the prior distribution. The ranges of these chosen parameters are defined according to a rough estimation on the experimental results and the prior knowledge. In Table 2, the random variables corresponding to $\boldsymbol{\vartheta}^{\text{ve}}$ and their uniform distribution ranges used to build the prior distributions are listed. The values of G_i and K_i, $(i = 1, .., 8)$ can vary respectively from 0.1 to 31000 MPa. In order to make the values of G_i and K_i have equal probability at different order of magnitude during random walk, and be possible to reach zero, their logarithm in base 10, noted lg, are used as the random variables with uniform distributions. The same treatment is also applied on g_1 and k_1 to make their random variables have equal probability in the ranges $[1, 10]$ s, $[10, 100]$ s and $[100, 1000]$ s during the random walk.

Table 2: The prior uniform distribution ranges of the visco-elastic material parameters.

$\boldsymbol{\vartheta}^{\text{ve}}$	E_∞ [MPa]	ν_∞ [-]	$\lg G_i$, $\lg K_i$ [-]*, $(i = 1, .., 8)$	$\lg g_1$, $\lg k_1$ [−]**
Ranges	$[800 \sim 1600]$	$[0.25 \sim 0.45]$	$[-1 \sim 4.5]$	$[0.0 \sim 3.0]$

* G_i and K_i are in MPa unit; ** g_1 and k_1 are in s unit.

Visco-Plastic (VP) parameters $\boldsymbol{\vartheta}^{vp}$. The parameters are the viscous parameters η and s in Eq. (12), the yield parameter α in Eq. (18), initial tensile and compressive yield stresses σ_{t}^0 and σ_{c}^0, flow potential parameter β in Eq. (19), and hardening parameters t_0, H_{t}^0, h_{t} and c_0, H_{c}^0, h_{c} respectively in Eqs. (25) and (26) for tensile and compressive cases. There is a total of 12 visco-plastic material parameters that need to be identified. Because of $\sigma_{\text{t}}^0 = m^0\sigma_{\text{c}}^0$, the parameters m^0 and σ_{c}^0 are used in the identification process. The adopted random variables and their uniform distribution ranges are listed in Table 3 for the construction of prior distribution. The logarithm form is also applied for the random parameters η, t_0, c_0, H_{t}^0 and H_{c}^0 for the same reason as that for the visco-elastic parameters.

Subset of parameters $\underline{\boldsymbol{\vartheta}} \subset \boldsymbol{\vartheta}$ *for SBI.* During the SBI, a group of N_{p} material parameters $\underline{\boldsymbol{\vartheta}} = [\vartheta_1, \vartheta_2, ..., \vartheta_{N_{\text{p}}}]$ which is a subset of $\boldsymbol{\vartheta}$, is considered. This subset $\underline{\boldsymbol{\vartheta}}$ can be part of the VE parameters (or the whole VE set), part of the VP parameters (or the whole VP set), or a combination of both, as this will be discussed in Section 4.2.3.

Table 3: The prior uniform distribution ranges of the visco-plastic material parameters.

$\boldsymbol{\vartheta}^{\mathrm{vp}}$	$\lg \eta$ [-]*	s [-]	α [-]	β [-]	
Ranges	$[3.0 \sim 5.3]$	$[0.01 \sim 0.5]$	$[1.0 \sim 7.0]$	$[0.0 \sim 2.0]$	
$\boldsymbol{\vartheta}^{\mathrm{vp}}$	σ_{c}^0 [MPa]	m^0 [-]	$\lg t_0$, $\lg c_0$ [-]**	$\lg H_{\mathrm{t}}^0$, $\lg H_{\mathrm{c}}^0$ [-]***	h_{t}, h_{c} [-]
Ranges	$[5.0 \sim 60.0]$	$[0.1 \sim 0.9]$	$[-5.0 \sim 3.0]$	$[-3 \sim 2.0]$	$[0 \sim 10000]$

* η is in MPa$\cdot$s unit;

** t_0 and c_0 are in MPa unit;

*** H_{t}^0 and H_{c}^0 are in MPa unit.

The prior distribution of $\underline{\boldsymbol{\vartheta}}$ is constructed from N_{p} independent distributions, as

$$\pi_{\mathrm{prior}}(\underline{\boldsymbol{\vartheta}}) = \prod_{i=1}^{N_{\mathrm{p}}} \mathcal{U}^{\vartheta_i} \,, \tag{45}$$

where $\mathcal{U}$ refers to a uniform distribution and the bounds of these uniform distributions are presented in Tables 2 and 3. Concerning the random variable ς, which relates to the standard deviation in Eq. (40), it also has an uniform prior distribution

$$\pi_{\mathrm{prior}}(\varsigma) = \mathcal{U}_{(0.03,\,0.15)} \,. \tag{46}$$

Since a uniform distribution is used as prior distribution for all the random parameters, the value of $\pi_{\mathrm{prior}}(\underline{\boldsymbol{\vartheta}})$ in Eq. (45) will be constant as soon as all the parameters realizations stay in their ranges. Therefore a simplified treatment, such as

$$\pi_{\mathrm{prior}}(\underline{\boldsymbol{\vartheta}}) = \begin{cases} 1\,, & \text{for all the parameters falling in their ranges}\,, \\ 0\,, & \text{otherwise}\,, \end{cases} \tag{47}$$

can be used and the results of the MCMC random walk will not be affected. It needs to be noticed that the logarithm operations on some parameters have no effect on their prior distribution.

4.2.3. Experimental observations with data augmentation and SBI

In this section, we use the data of "V" specimens to detail the BI material parameter identification process of SLS printed PA12. The data for "H" specimens are presented in Appendix A to avoid a redundant description. The information of one observation, includes the experiment type, the engineering strain ε, the strain rate $\dot{\varepsilon}$, the observation time t for the relaxation test and the corresponding stress Σ. The observations are taken from the strain-stress curves of uniaxial tensile, compressive and relaxation tests of PA12 samples, and noted by $\boldsymbol{\beta}$. The experimental strain-stress curves are plotted in Fig. 5, and the picked observation points are marked on these curves. Since each observation corresponds to one loading condition at a given strain state, for repeated experiments, their averaged results are used as observations. In Fig.

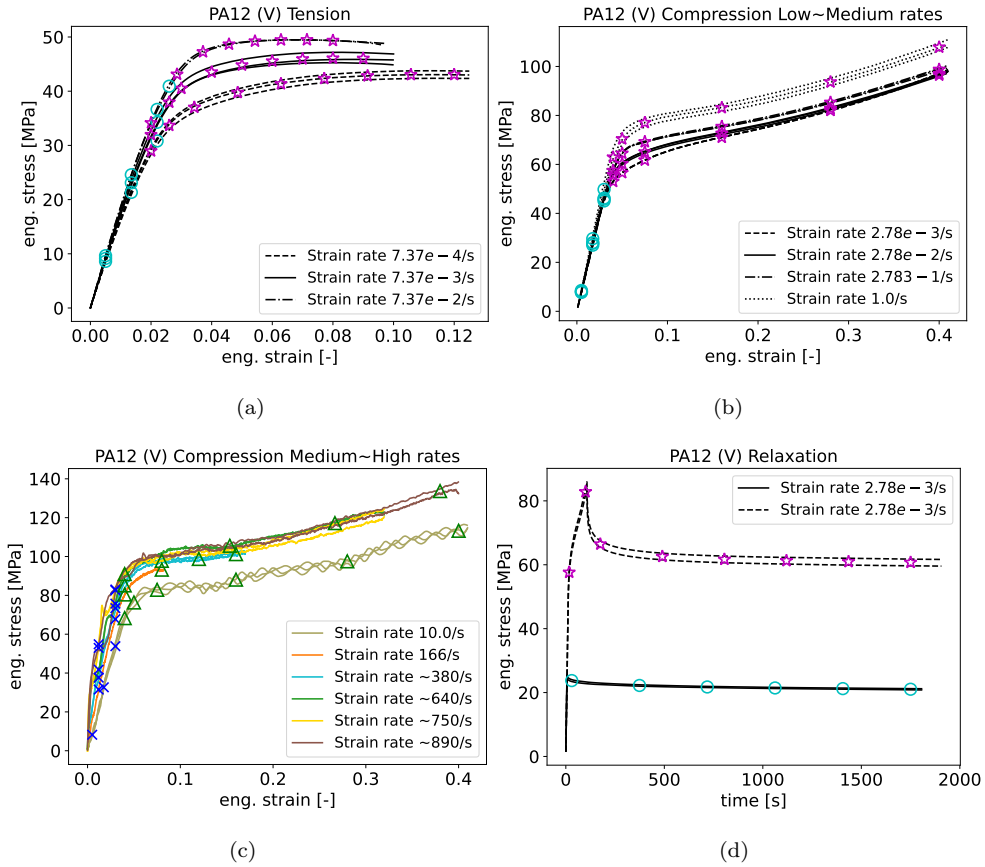

Figure 5: The experimental strain-stress curves of the "V" specimens and the picked observation points to conduct the Bayesian inference in (a) Tension; (b) and (c) Compression at low, medium and high loading rates respectively; and (d) Compression and relaxation tests.

5, 27 observations are marked with cyan circles and 18 with blue crosses for the visco-elastic stage, and 59 with magenta stars and 16 with green triangles for the visco-plastic stage; the discrimination of the color codes in explained here below.

The visco-elastic stage is the part of deformation history before initial yield stress is reached. The yield stress in the laboratory is defined by the true stress at the observed maximum tension [40]. The yield stress is chosen in [41] as the measured tension at a strain which corresponds closely to the observed first peak in the stress-strain response, for those samples that show a maximum, which could reach values up to 20% for specific material such as amorphous poly-ethylene. However, the exponential decay relaxation modulus, in Eqs. (8) and (9), is not able to describe the observed nonlinear response of samples before the physical yield point. Hence, the part of the experiment curves before an obvious non-linearity occurs is used here as the visco-elastic stage.

Since we have much less tension tests than that of compression, the compression observations would be

dominating the likelihood function and "win" the competition when inferring the pressure related parameters of the visco-plastic stage if we choose the same number of observations for each set of experiment. This would result in poor predictions for the tension test with the identified parameters. Therefore, during the visco-plastic stage, we take more observations from each set of tension tests than for compression tests in order to balance their weights in the likelihood function, i.e. among the 59 magenta starts, there are 27 observations from the tension tests at 3 different strain rates, 24 from the compression tests at 4 different strain rates and 8 from the relaxation test, see Fig. 5.

The material parameters to be inferred include respectively 20 visco-elastic and 12 visco-plastic parameters, see Tables 2 and 3, respectively. Hence, there are totally 32 random parameters and 120 observations that will be used in the BI. If one wants to use all the observation data at once to infer the material parameters all together, the resulting low values of the likelihood function will lead to a rather slow convergence of the MCMC random walk. Therefore, the BI process will be carried out in a sequence way in this work. The likelihood function constructed from the observations acts as a constraint on the MCMC random walk. In order to have all the possible combinations of material parameters being explored, the tested random samples of the parameters need to be wide enough during the random walk, although only those with a relatively high likelihood are kept. Therefore, for each BI sequence, we require at least 20000 parameters samples to be kept, which are only a small portion of the total explored samples during the random walk. Also, in order to avoid the previous BI sequence to introduce a bias in the following one, the observations used in each BI sequence need to be picked in a proper order: the observations which form a loose likelihood constraint will be applied first, and the tighter ones later, see A and B in Fig. 1(a). The observations which lead to a competition mechanism on the parameters need to be used together in a single BI sequence, see A and B in Fig. 1(b).

For this SBI, the material parameters and observations are divided into groups according to the correlation between the material parameters and observations.

- Firstly, since the visco-plastic properties have no effect on the visco-elastic response of the material, it is natural to divide the material parameters and observations into visco-elastic and visco-plastic groups:

$$\boldsymbol{\vartheta} = [\boldsymbol{\vartheta}^{\mathrm{ve}}, \boldsymbol{\vartheta}^{\mathrm{vp}}], \text{ and } \boldsymbol{\beta} = [\boldsymbol{\beta}^{\mathrm{ve}}, \boldsymbol{\beta}^{\mathrm{vp}}]\,. \tag{48}$$

- Secondly, the observation data of the visco-elastic and visco-plastic groups are both further divided into two parts,

$$\boldsymbol{\beta}^{\mathrm{ve}} = [\boldsymbol{\beta}_1^{\mathrm{ve}}, \boldsymbol{\beta}_2^{\mathrm{ve}}], \text{ and } \boldsymbol{\beta}^{\mathrm{vp}} = [\boldsymbol{\beta}_1^{\mathrm{vp}}, \boldsymbol{\beta}_2^{\mathrm{vp}}]\,, \tag{49}$$

  where $\boldsymbol{\beta}_1^{\mathrm{ve}}$ and $\boldsymbol{\beta}_1^{\mathrm{vp}}$ correspond to the observations of the low strain rate tests, and $\boldsymbol{\beta}_2^{\mathrm{ve}}$ and $\boldsymbol{\beta}_2^{\mathrm{vp}}$ correspond to the observations of the high strain rate tests. In Fig. 5, these observations are marked with cyan circles for $\boldsymbol{\beta}_1^{\mathrm{ve}}$, blue crosses for $\boldsymbol{\beta}_2^{\mathrm{ve}}$, magenta stars for $\boldsymbol{\beta}_1^{\mathrm{vp}}$, and green triangles for $\boldsymbol{\beta}_2^{\mathrm{vp}}$.

The SBI process is performed in four steps, and at each step a BI with reduced observations and/or random parameters is carried out. The used observations, inferred parameters and their prior distribution, likelihood function and posterior distributions of those sub-BI are listed in Table 4.

Table 4: Material parameters and used observations in the sequential Bayesian inference.

Visco-Elastic parameters $\boldsymbol{\vartheta}^{\mathrm{ve}}$		
BI step	I	II
Observations	$\boldsymbol{\beta}_1^{\mathrm{ve}}$, cyan circles	$\boldsymbol{\beta}_2^{\mathrm{ve}}$, blue crosses
Likelihood	$\pi\left(\boldsymbol{\beta}_1^{\mathrm{ve}}\middle\vert\boldsymbol{\vartheta}^{\mathrm{ve}}, \varsigma\right)$	$\pi\left(\boldsymbol{\beta}_2^{\mathrm{ve}}\middle\vert\boldsymbol{\vartheta}^{\mathrm{ve}}, \varsigma\right)$
Prior	$\pi_{\mathrm{prior}}\left(\boldsymbol{\vartheta}^{\mathrm{ve}}\right)\pi_{\mathrm{prior}}\left(\varsigma\right)$	$\pi_{\mathrm{post}}\left(\boldsymbol{\vartheta}^{\mathrm{ve}}, \varsigma\middle\vert\boldsymbol{\beta}_1^{\mathrm{ve}}\right)$
Posterior	$\pi_{\mathrm{post}}\left(\boldsymbol{\vartheta}^{\mathrm{ve}}, \varsigma\middle\vert\boldsymbol{\beta}_1^{\mathrm{ve}}\right)$	$\pi_{\mathrm{post}}\left(\boldsymbol{\vartheta}^{\mathrm{ve}}, \varsigma\middle\vert\boldsymbol{\beta}^{\mathrm{ve}}\right)$
Visco-Plastic parameters $\boldsymbol{\vartheta}^{\mathrm{vp}}$		
BI step	III	IV
Observations	$\boldsymbol{\beta}_1^{\mathrm{vp}}$, magenta stars	$\boldsymbol{\beta}_2^{\mathrm{vp}}$, green triangles
Likelihood	$\pi\left(\boldsymbol{\beta}_1^{\mathrm{vp}}\middle\vert\boldsymbol{\vartheta}^{\mathrm{ve}}, \boldsymbol{\vartheta}^{\mathrm{vp}}, \varsigma\right)$	$\pi\left(\boldsymbol{\beta}_2^{\mathrm{vp}}\middle\vert\boldsymbol{\vartheta}^{\mathrm{ve}}, \boldsymbol{\vartheta}^{\mathrm{vp}}, \varsigma\right)$
Prior	$\pi_{\mathrm{prior}}\left(\boldsymbol{\vartheta}^{\mathrm{vp}}\right)\pi_{\mathrm{post}}\left(\boldsymbol{\vartheta}^{\mathrm{ve}}, \varsigma\middle\vert\boldsymbol{\beta}^{\mathrm{ve}}\right)$	$\pi_{\mathrm{post}}\left(\boldsymbol{\vartheta}^{\mathrm{ve}}, \boldsymbol{\vartheta}^{\mathrm{vp}}, \varsigma\middle\vert\boldsymbol{\beta}^{\mathrm{ve}}, \boldsymbol{\beta}_1^{\mathrm{vp}}\right)$
Posterior	$\pi_{\mathrm{post}}\left(\boldsymbol{\vartheta}^{\mathrm{ve}}, \boldsymbol{\vartheta}^{\mathrm{vp}}, \varsigma\middle\vert\boldsymbol{\beta}^{\mathrm{ve}}, \boldsymbol{\beta}_1^{\mathrm{vp}}\right)$	$\pi_{\mathrm{post}}\left(\boldsymbol{\vartheta}^{\mathrm{ve}}, \boldsymbol{\vartheta}^{\mathrm{vp}}, \varsigma\middle\vert\boldsymbol{\beta}^{\mathrm{ve}}, \boldsymbol{\beta}^{\mathrm{vp}}\right)$

4.2.4. Posterior distribution

Using the formalism (33) and (34), the posterior distributions of the SBI,

$$\pi_{\mathrm{post}}\left(\boldsymbol{\vartheta}^{\mathrm{ve}}\middle\vert\boldsymbol{\beta}_1^{\mathrm{ve}}\right) \propto \pi\left(\boldsymbol{\beta}_1^{\mathrm{ve}}\middle\vert\boldsymbol{\vartheta}^{\mathrm{ve}}\right)\pi_{\mathrm{prior}}\left(\boldsymbol{\vartheta}^{\mathrm{ve}}\right), \tag{50}$$

$$\pi_{\mathrm{post}}\left(\boldsymbol{\vartheta}^{\mathrm{ve}}\middle\vert\boldsymbol{\beta}^{\mathrm{ve}}\right) \propto \pi\left(\boldsymbol{\beta}_2^{\mathrm{ve}}\middle\vert\boldsymbol{\vartheta}^{\mathrm{ve}}\right)\pi_{\mathrm{post}}\left(\boldsymbol{\vartheta}^{\mathrm{ve}}\middle\vert\boldsymbol{\beta}_1^{\mathrm{ve}}\right), \tag{51}$$

$$\pi_{\mathrm{post}}\left(\boldsymbol{\vartheta}^{\mathrm{ve}}, \boldsymbol{\vartheta}^{\mathrm{vp}}\middle\vert\boldsymbol{\beta}^{\mathrm{ve}}, \boldsymbol{\beta}_1^{\mathrm{vp}}\right) \propto \pi\left(\boldsymbol{\beta}_1^{\mathrm{vp}}\middle\vert\boldsymbol{\vartheta}^{\mathrm{ve}}, \boldsymbol{\vartheta}^{\mathrm{vp}}\right)\pi_{\mathrm{prior}}\left(\boldsymbol{\vartheta}^{\mathrm{vp}}\right)\pi_{\mathrm{post}}\left(\boldsymbol{\vartheta}^{\mathrm{ve}}\middle\vert\boldsymbol{\beta}^{\mathrm{ve}}\right), \tag{52}$$

$$\pi_{\mathrm{post}}\left(\boldsymbol{\vartheta}^{\mathrm{ve}}, \boldsymbol{\vartheta}^{\mathrm{vp}}\middle\vert\boldsymbol{\beta}^{\mathrm{ve}}, \boldsymbol{\beta}^{\mathrm{vp}}\right) \propto \pi\left(\boldsymbol{\beta}_2^{\mathrm{vp}}\middle\vert\boldsymbol{\vartheta}^{\mathrm{ve}}, \boldsymbol{\vartheta}^{\mathrm{vp}}\right)\pi_{\mathrm{post}}\left(\boldsymbol{\vartheta}^{\mathrm{ve}}, \boldsymbol{\vartheta}^{\mathrm{vp}}\middle\vert\boldsymbol{\beta}^{\mathrm{ve}}, \boldsymbol{\beta}_1^{\mathrm{vp}}\right), \tag{53}$$

are evaluated using a MCMC technique, which corresponds to a random walk in the parameter space $\underline{\boldsymbol{\vartheta}} \in \mathbb{R}^{N_{\mathrm{p}}}$, where $\underline{\boldsymbol{\vartheta}} = \boldsymbol{\vartheta}^{\mathrm{ve}}$ for the first two BI steps and $\underline{\boldsymbol{\vartheta}} = \boldsymbol{\vartheta}$ for the last two BI steps, with $N_{\mathrm{p}} = 21$, 21, 33 and 33 respectively, as summarized in Fig. 6. The adaptive variant [42] of the Metropolis algorithm [43] is used, see also [29] for details. Although the convergence has been reached after a few thousands of samples at beginning of MCMC random walk, we have generated more than 20000 samples in each BI step, from which the first 2000 samples of each random walk are always discarded. Indeed, since the initial point of the walk has always effect on the sampling results, in particular on the first ones, the latter have to be discarded to remove this bias.

Following the flowchart of Fig. 6, a criterion $\pi_{\mathrm{prior}}(\underline{\boldsymbol{\vartheta}}_p) > p_{\mathrm{prior}}^{\mathrm{th}}$ is evaluated first for each new sample. In the first BI step, it is set that $p_{\mathrm{prior}}^{\mathrm{th}} = 0$ to guarantee that the new samples are within the uniform

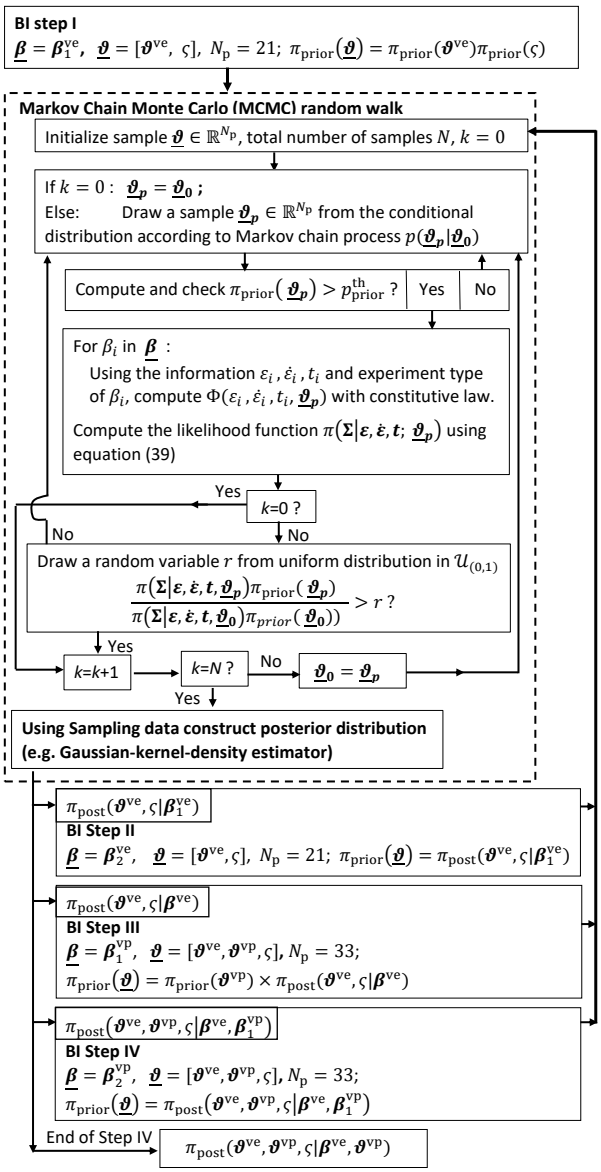

Figure 6: Flowchart of the adopted SBI process for the VE-VP parameter identification of SLS printed PA12 material.

distribution range defined by their prior. Using the data from the MCMC random walk during the previous BI step, a Gaussian-kernel-density estimator is constructed, see Appendix B, and the probability of all these data is evaluated by this estimator. The minimum value of their probability is used to define the $p_{\mathrm{prior}}^{\mathrm{th}}$ in the following BI step, to make sure that the MCMC random walk stays within the prior distribution range, as the obtained Gaussian-kernel-density estimator is also used to evaluate the $\pi_{\mathrm{prior}}(\underline{\boldsymbol{\vartheta}}_{\boldsymbol{p}})$ in the following BI step. In practice, the typical value of $p_{\mathrm{prior}}^{\mathrm{th}} \sim 10^{-6}$ for the 2nd, 3rd and 4th BI steps is used in this work.

5. Parameters of SLS printed PA12 identified by SBI

In this section, the final results of the SBI are presented for the "V" and "H" specimens of SLS printed PA12, respectively. The definition of "V" and "H" relates to the printing direction of the specimens, see the illustration in Fig. 3.

5.1. The maximum a-posteriori (MAP) estimates of visco-elastic parameters

Table 5: The MAP estimates of the visco-elastic material parameters of the "V" specimen.

$\boldsymbol{\vartheta}^{\text{ve}}$	E_∞ [MPa]	ν_∞ [-]	g_1 [s]	k_1 [s]				
Value	1366.7	0.278	7.36	9.12				
G_i	G_1	G_2	G_3	G_4	G_5	G_6	G_7	G_8
[MPa]	0.33	27.23	18.55	1.62	21.66	9.91	1722.24	6.13
K_i	K_1	K_2	K_3	K_4	K_5	K_6	K_7	K_8
[MPa]	28281.49	0.30	747.17	467.82	0.51	7874.44	39.13	2422.40

Table 6: The MAP estimates of the visco-elastic material parameters of the "H" specimen.

$\boldsymbol{\vartheta}^{\text{ve}}$	E_∞ [MPa]	ν_∞ [-]	g_1 [s]	k_1 [s]				
Value	1195.14	0.276	2.83	14.09				
G_i	G_1	G_2	G_3	G_4	G_5	G_6	G_7	G_8
[MPa]	26.75	71.53	8.26	10.73	145.03	6.00	1655.17	4.61
K_i	K_1	K_2	K_3	K_4	K_5	K_6	K_7	K_8
[MPa]	1134.86	1.25	265.16	58.64	2605.61	26.10	3849.62	2469.14

The maximum a-posteriori (MAP) estimates of the visco-elastic-visco-plastic material parameters can be extracted directly from the MCMC random walk result of the 4^{th} BI step. The obtained visco-elastic parameters are respectively reported in Tables 5 and 6 for the "V" and "H" specimens.

From Tables 5 and 6, it can be seen that the stiffness of the "V" specimens is higher than for the "H" specimens in general. The two kinds of specimens have similar infinite Poisson's ratio, which is around 0.28. In this work, the Poisson's ratio is also a function of time since we deal with the visco-elastic shear and bulk moduli separately. According to the listed shear and bulk moduli in Tables 5 and 6, the instant Poisson's ratio is higher than its infinite value.

A few of the visco-elastic shear and bulk moduli have much lower values compared to the others, such as G_1, G_4, K_2, K_5 in Table 5 and K_2 in Table 6. These terms with rather low values indicate their negligible effect in the visco-elastic response of the material. Therefore, the material parameters could be reduced by pruning these terms from the Maxwell model without loosing accuracy in the numerical analysis.

5.2. The maximum a-posteriori (MAP) estimates of the visco-plastic parameters

Table 7: The MAP estimates of the visco-plastic material parameters of the "V" specimen.

$\boldsymbol{\vartheta}^{\mathrm{vp}}$	η [MPa · s]	s [-]	α [-]	β [-]
Value	1.33×10^5	0.18	3.63	0.18
$\boldsymbol{\vartheta}^{\mathrm{vp}}$	σ_{c}^0 [MPa]	c_0 [MPa]	H_{c}^0 [MPa]	h_{c} [-]
Value	30.04	7.85×10^{-3}	14.41	296.38
$\boldsymbol{\vartheta}^{\mathrm{vp}}$	m^0 [-]	t_0 [MPa]	H_{t}^0 [MPa]	h_{t} [-]
Value	0.80	146.34	5.24×10^{-4}	9955.79

Table 8: The MAP estimates of the visco-plastic material parameters of the "H" specimen.

$\boldsymbol{\vartheta}^{\mathrm{vp}}$	η [MPa · s]	s [-]	α [-]	β [-]
Value	3037.09	0.115	1.82	0.076
$\boldsymbol{\vartheta}^{\mathrm{vp}}$	σ_{c}^0 [MPa]	c_0 [MPa]	H_{c}^0 [MPa]	h_{c} [-]
Value	35.95	0.55	0.30	6938.03
$\boldsymbol{\vartheta}^{\mathrm{vp}}$	m^0 [-]	t_0 [MPa]	H_{t}^0 [MPa]	h_{t} [MPa]
Value	0.29	0.032	0.0195	590.01

The MAP estimates of the visco-plastic material parameters, extracted from the MCMC random walk result of the final BI step, are respectively reported in tables 7 and 8 for the "V" and "H" specimens.

From Tables 7 and 8, we can see that the visco-plastic parameters of the "V" and "H" specimens are quite different. It is mainly because the "H" specimens have a higher porosity than the "V" specimens, and this high porosity leads to lower mechanical performance of the "H" specimen in tension, see Figs. 5(a) and 14(a) presented in Appendix A. Since a pressure associated plasticity is adopted in our modeling approach, the results of the tension tests have an important effect in the visco-plastic parameters identification.

5.3. The distributions and correlations of the VE-VP material parameters

Although the MAP estimate of the material parameters is the best result ever reached during the MCMC random walk, it is not obviously much more accurate than the other parameter sets obtained during the random walk. The advantage of the BI is not to provide a set of optimized material parameters, but to explore the feasible parameter sets by evaluating their probability, or distribution. This statistical information is carried by the massive data resulting from the MCMC random walk, under the form of realizations of the material parameter set $\boldsymbol{\vartheta}$. In Fig. 7, the joint distributions of 8 out of 32 material parameters are plotted by 2D histograms, with more figures for the joint and marginal distributions for "V" and "H" specimens being provided in Appendix C.1 and Appendix C.2, respectively. Fig. 7 shows that correlations exist between

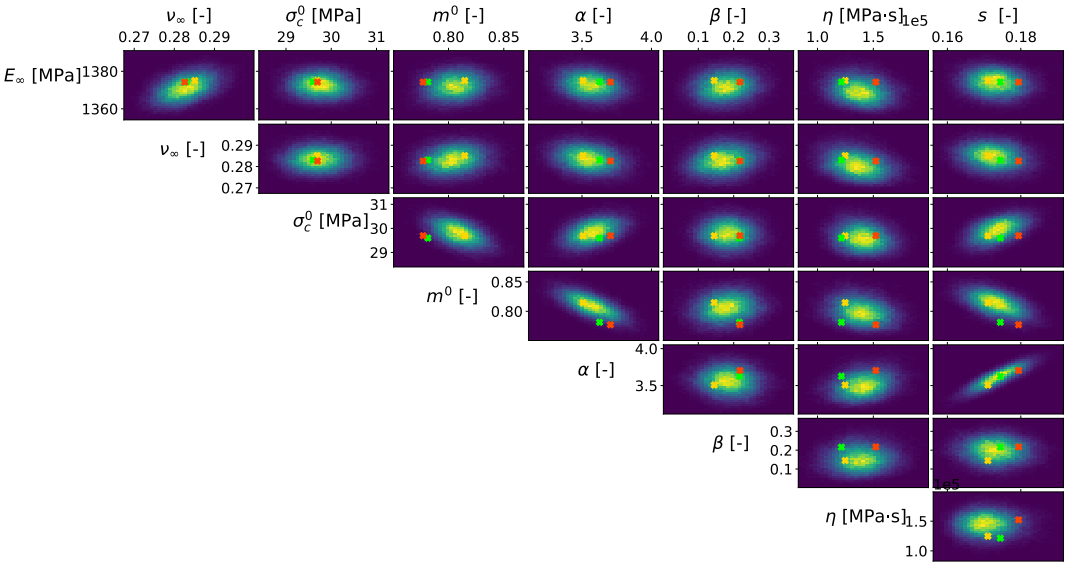

(a)

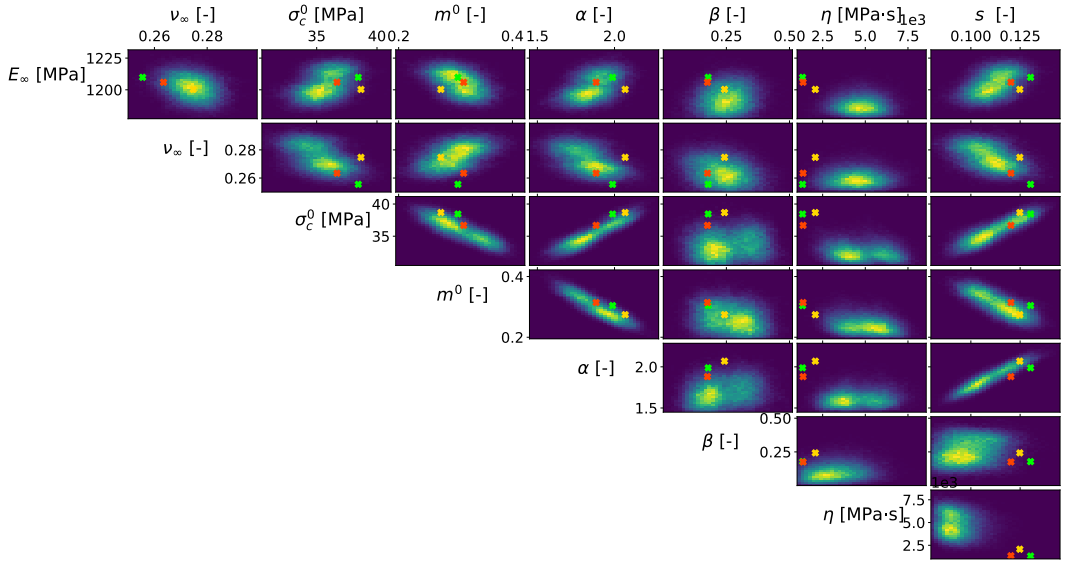

(b)

Figure 7: The random material parameters distributions for the "V" specimens (a) and "H" specimens (b). The marked parameter points correspond to the numerical results (with the same colors) reported in Figs. 8 and 9, respectively. Yellow and blue colors indicate respectively high and low probability density in the parameter space.

all the parameter pairs in general, and strong correlations can be seen between some parameter pairs, such σ_c^0 and m^0, α and s.

Three randomly picked material parameter points are marked in Figs. 7(a) and 7(b) respectively for the "V" and "H" specimens. Considering successively these three sets $\boldsymbol{\vartheta}$ of material parameters, the mechanical

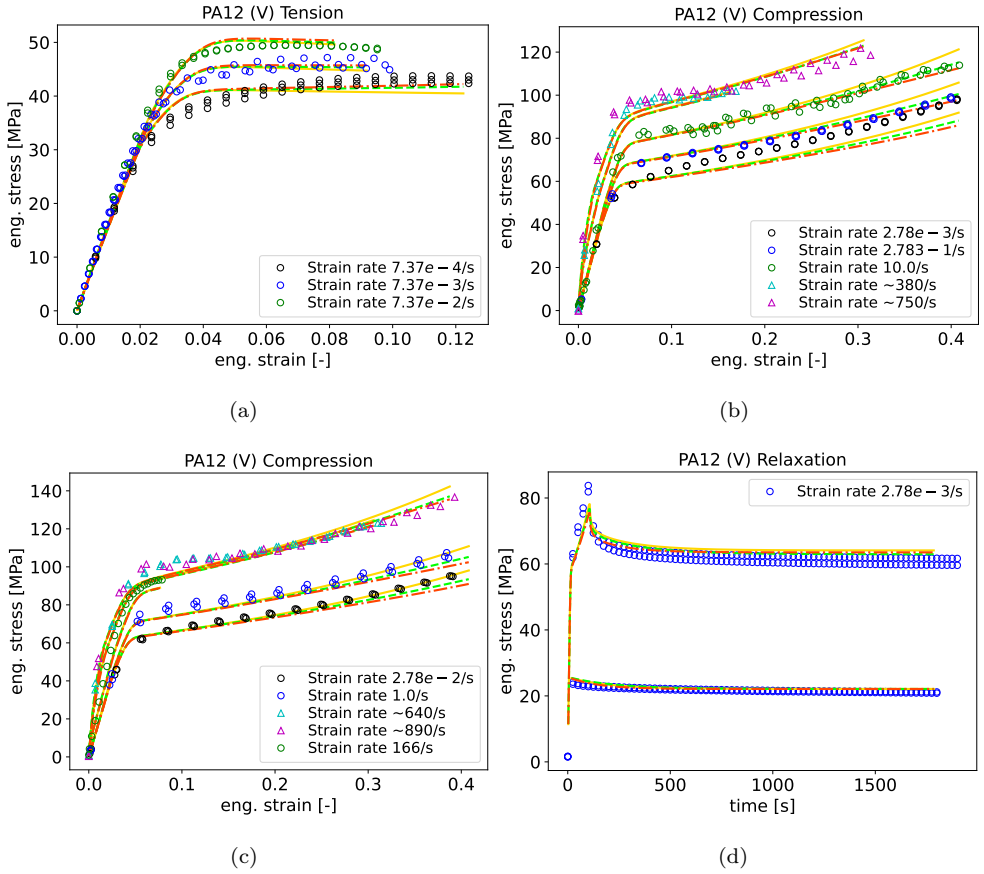

Figure 8: The engineering strain-stress curves of the "V" specimens with the corresponding material parameter points (with the same colors) marked in Fig. 7(a). The numerical results are presented by lines and the experimental results by markers.

responses of the studied materials are simulated for the different studied experimental loading conditions. The numerical results are plotted in Figs. 8 and 9, together with the experimental strain-stress curves for comparison. It can be seen that with the adopted visco-elastic-visco-plastic constitutive model, all these sets of material parameters yield fair predictions for each loading case. Although some sets of parameters have shown better performance under certain loading conditions, there is not a parameter set which fits all the experimental results perfectly. This may be because of the limitation of adopted material constitutive model, combined to the various uncertainties and errors due to the experimental tests that use different testing machines. Moreover, with different parameters sets, a certain degree of discrepancy among their numerical results is exactly what we expected from BI.

The data related to the MCMC random walks are available in [44]. We however note that the inferred values of β from the uniaxial tests can make the visco-elastic-visco-plastic material model resolution difficult when solving 3D complex problems. For such simulations, β can be increased by 50% from the inferred values without affecting the uniaxial test predictions while making the local convergence of the material

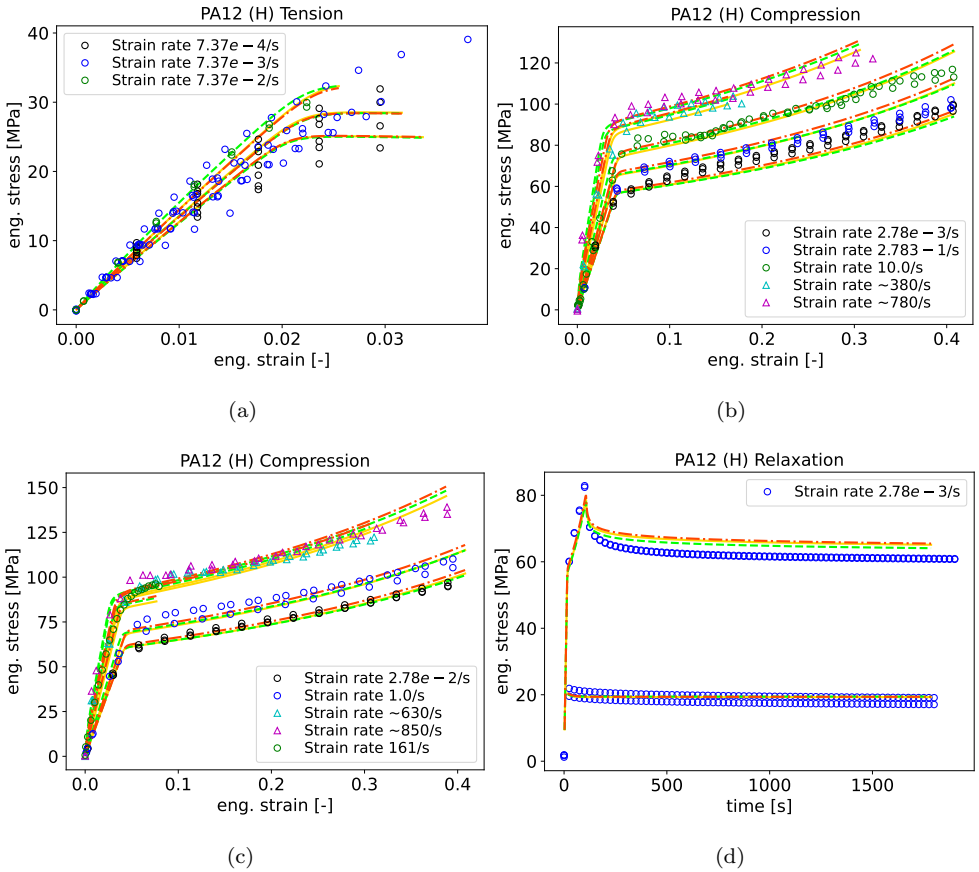

Figure 9: The engineering strain-stress curves of the "H" specimens with the corresponding material parameter points (with the same colors) marked in Fig. 7(b). The numerical results are presented by lines and the experimental results by markers.

model faster.

6. Random material parameters generation with a Generative Adversarial Network (GAN)

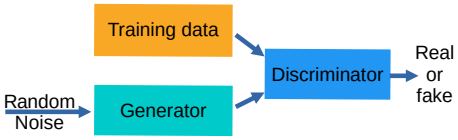

Figure 10: Illustration of a Generative Adversarial Network.

Using the data obtained from the MCMC random walk, a Generative Adversarial Network (GAN) is trained to generate new random material parameters. In a GAN, a NNW is taught to capture the training data's distribution, so that new data can be generated following the same distribution. A GAN is made of two distinct models, a generator and a discriminator, as illustrated in Fig. 10. The task of the generator is

to produce "fake" data that look like the training data, while the task of the discriminator is to check, from generated data and training data, whether or not the data are real training data or "fake" data coming from the generator. During the training, the generator is trained to trick the discriminator by generating better and better fakes, while the discriminator is trained to correctly classify the real and fake data.

6.1. Generation of parameters with uni-modal distribution

In this work, two Feed-forward Neural Networks (FNN) are adopted for both the generator and the discriminator. The architecture of a FNN is represented by $\{Input_{\text{size}}, Hidden^1_{\text{size}}, ... Hidden^n_{\text{size}}, Output_{\text{size}}\}$, where $Input_{\text{size}}$ and $Output_{\text{size}}$ are respectively the dimensions of input and output, $Hidden^i_{\text{size}}$, $i = 1, ..., n$ are the dimension of the n hidden layers. The architectures

$$\text{Generator}: \{32, 60, 60, 60, 32\}_{\text{V}}, \quad \text{Discriminator}: \{32, 60, 60, 60, 1\}_{\text{V}}, \tag{54}$$

are used for the material properties of the "V" specimens, which exhibit a uni-modal distribution as shown in Fig. 7(a). LeakyReLU is used for activation functions for the input and hidden layers, while a hyperbolic tangent function (tanh) and a sigmoid function are used for the output layers of generator and discriminator, respectively.

6.2. Generation of parameters with bi-modal distribution

In this section, we focus on the random material parameter generation of "H" specimen whose BI identified parameters have shown a bi-modal distribution, as shown in Fig. 7(b). This bi-modal distribution, $\pi(\boldsymbol{\vartheta})$, can be treated as a mixture of two uni modal distributions following

$$\pi(\boldsymbol{\vartheta}) = (1-p)\pi_0(\boldsymbol{\vartheta}) + p\pi_1(\boldsymbol{\vartheta}), \tag{55}$$

where p is the mixing parameter, which is estimated using the data resulting from the MCMC random walk. To this end, a clustering operation is first performed on these data, $\mathcal{D}$, to classify them into two groups, $\mathcal{D}_0$ and $\mathcal{D}_1$, where $\mathcal{D} = \mathcal{D}_0 \cup \mathcal{D}_1$. Then the mixing parameter, p, is estimated by the ratio between the number of data in the first group, $\mathcal{D}_1$, with the total number of data in the whole data set $\mathcal{D}$.

Two generators of uni-modal distribution, $\pi_0(\boldsymbol{\vartheta})$ and $\pi_1(\boldsymbol{\vartheta})$ can be trained separately, using the data $\mathcal{D}_0$ and $\mathcal{D}_1$, respectively. During the random material parameter generation, a random number (0 or 1) is first generated from a Bernoulli distribution with its mean equals p. Then this number serves as an indicator to choose the corresponding generator, either $\pi_0(\boldsymbol{\vartheta})$ or $\pi_1(\boldsymbol{\vartheta})$, to sample the final parameters. The architectures

$$\text{Generator}: \{32, 200, 200, 200, 32\}_{\text{H}}, \quad \text{Discriminator}: \{32, 100, 100, 100, 1\}_{\text{H}}, \tag{56}$$

are adopted for the generators of both $\pi_0(\boldsymbol{\vartheta})$ and $\pi_1(\boldsymbol{\vartheta})$.

6.3. Training of the GAN

The Binary Cross Entropy loss (BCELoss) function is used to evaluate the output of the discriminator.

The training data of the discriminator are divided into two parts. The first part of the data is the set material parameter data obtained from the MCMC random walk. These data are normalized by feature to map their values into the $[-1, 1]$ range. Then the label "1.0" is set as their reference output of the discriminator for "real" data meaning. The second part is a set of independent Gaussian noises of dimension 32, which first pass the generator and produce the input for the discriminator, and are labeled as "0.0" as their reference output of the discriminator for "fake" data meaning.

Then, the training data of the generator is constituted by the independent Gaussian noises input and the label "1.0" is set as their reference output of discriminator for "real".

The learnable parameters of the discriminator and generator are updated alternately during the training.

6.4. Results

Using the trained random parameter generators, 100000 data points are generated for both the "V" and the "H" specimens. The joint distributions of a few picked parameters are plotted under the form of 2D histograms in Figs. 11, which have to be compared to Figs. 7. A good agreement can be found between the 2D histograms of the original data and of the generated data. The remaining 2D histograms of the generated data are reported in Appendix D

Three material parameter sets are randomly picked from the generated data for both the "V" and "H" specimens, and marked in Fig. 11(a) and Fig. 11(b), respectively. Numerical simulations are then performed for the different studied experimental loading conditions and are presented in Figs. 12 and 13. It can be seen that the numerical simulations with the generated material parameters can predict well the mechanical behaviors of the material under the different loading conditions. The numerical results obtained with the generated material parameter sets are shown to have the same accuracy with respect to the experimental curves as the simulations conducted with the original material data arising from the MCMC random walk.

7. Conclusions

In this work, the parameters of a finite-strain visco-elastic-visco-plastic formulation are inferred from experimental tests performed PA12 samples processed by SLS. The experimental tests comprise compressive and tensile loading tests at different strain rates ranging from $10^{-4}\,\mathrm{s}^{-1}$ to $10^{3}\,\mathrm{s}^{-1}$, as well as stress relaxation tests for two printing directions. The constitutive model comprises 32 material parameters.

Given the number of available observations and material parameters to be identified, a sequential Bayesian inference is suggested in which only a part of the observations and/or material parameters are considered at first in order to refine progressively the prior distributions to be used during the Markov

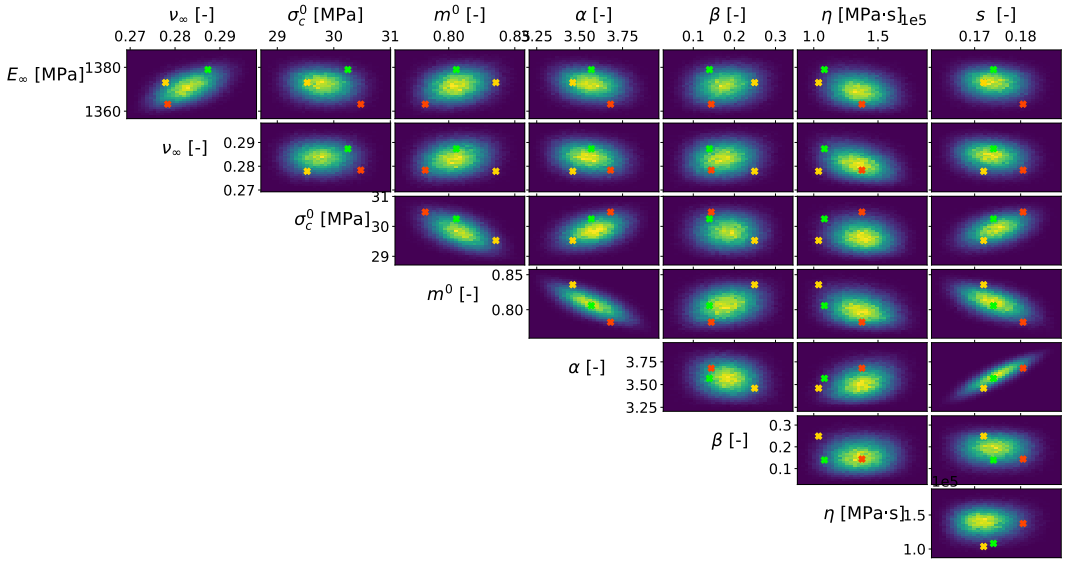

(a)

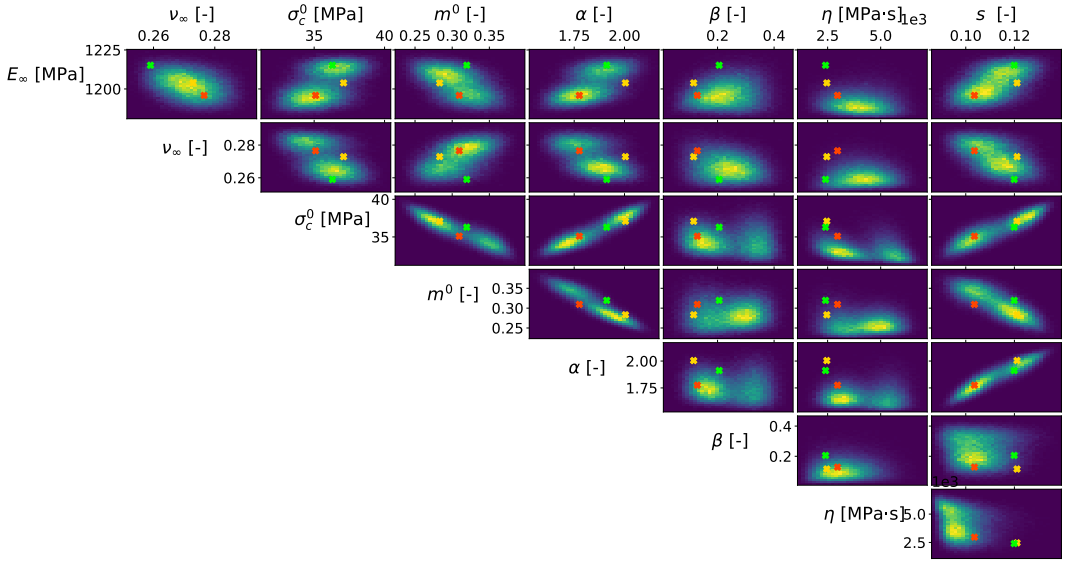

(b)

Figure 11: The generated random material parameters distributions for the "V" specimens (a) and "H" specimens (b). The marked parameter points correspond to the numerical results (with the same colors) reported in Figs. 12 and 13, respectively. Yellow and blue colors indicate respectively high and low probability density in the parameter space.

Chain Monte Carlo (MCMC) random walk by using the posterior distribution resulting from the previous BI step. The sets of observations and of material parameters are then enriched for the BI step. This SBI possesses the advantages of improving the inference efficiency since on the one hand the prior are not exaggeratedly wide in the subsequent steps and on the other hand the likelihood function does not yield

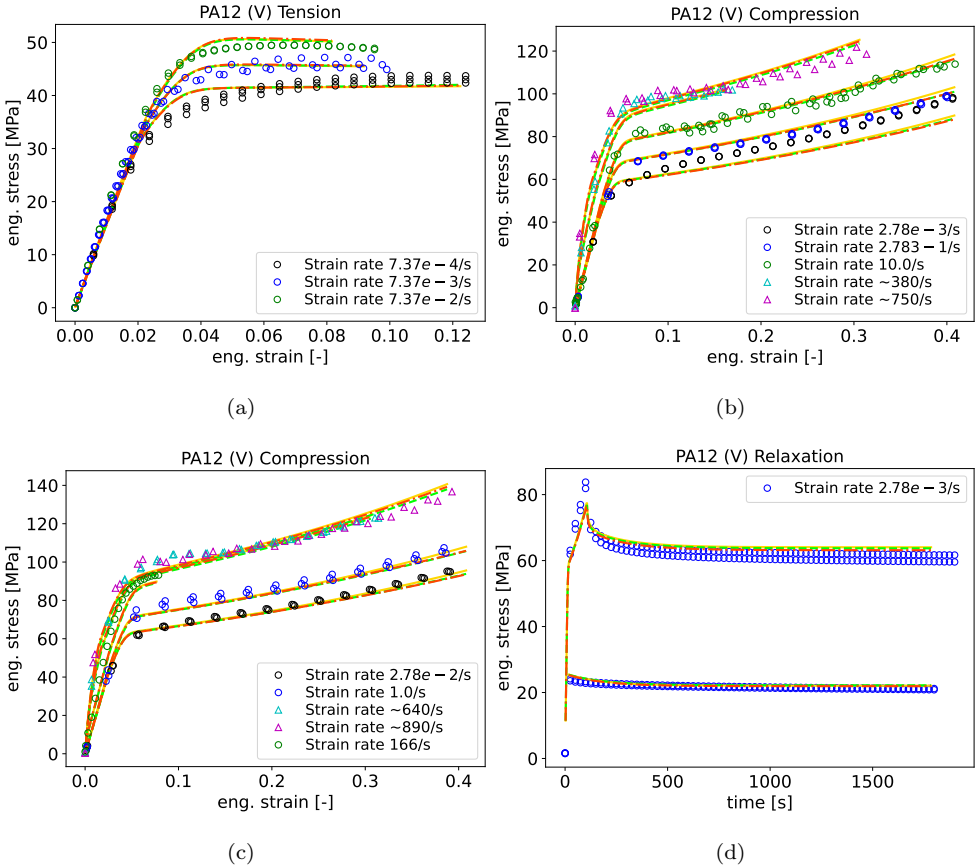

Figure 12: The engineering strain-stress curves of the "V" specimens with the generated material parameters (with the same colors) marked in Fig. 11(a). The numerical results are presented by lines and the experimental results by markers.

extremely low values as it would be the case when considering all the parameters and observation at once with large prior, hence improving the convergence when using Markov Chain Monte Carlo (MCMC) random walk to generate samples in high-dimensional parameter spaces. Besides, since the VE-VP model is pressure sensitive and discriminate between tension and compression in both the visco-elastic and visco-plastic ranges, it is important to have enough observations in both tensile and compressive cases not to overweight some tests. Therefore we have applied an observations augmentation of the tensile experimental tests.

The advantage of the BI over classical identification procedure is that it accounts for the errors in the experimental measurements but also for the model limitations by not trying to perfectly reproduced experimental curves. As a result, the BI yields realizations of the material model parameters and not a unique set of parameters. Although the maximum a-posteriori (MAP) estimates of the material properties can further be used, information on the experimental and model errors can be captured by considering the statistical content of the random vector of material parameter realizations arising from the MCMC random walk. In order to exploit this information in further analysis, a random material parameter generator is

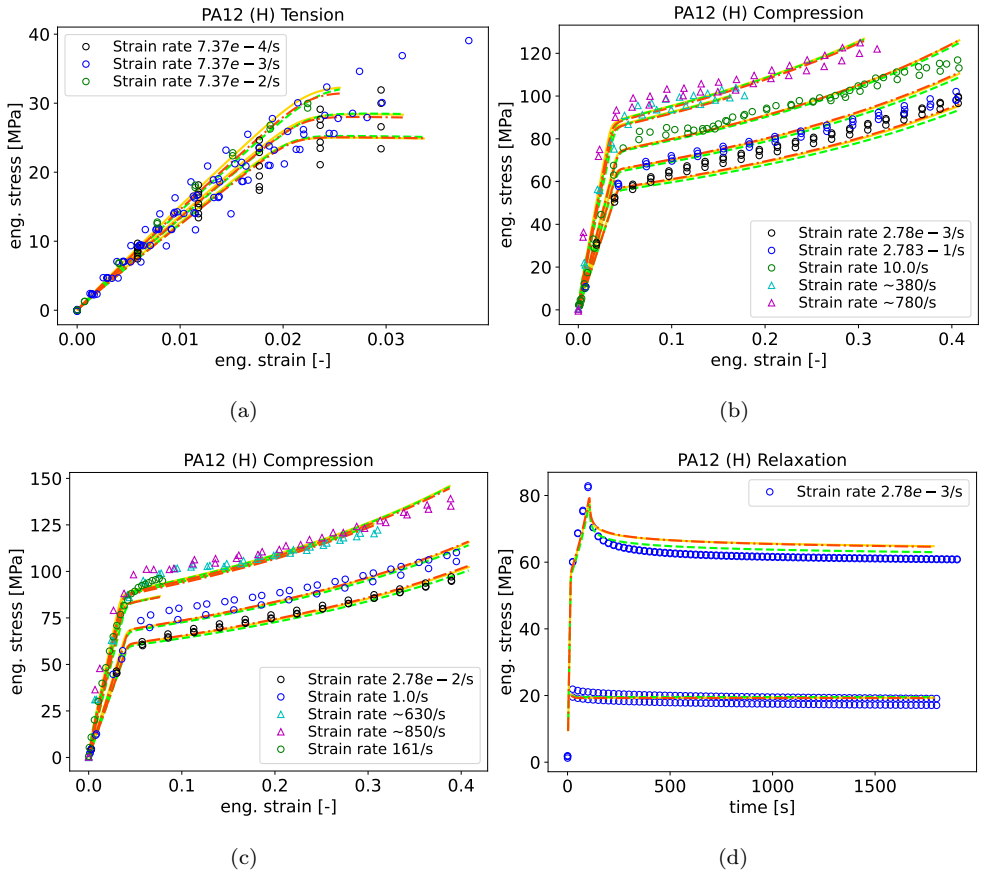

Figure 13: The engineering strain-stress curves of the "H" specimens with the generated material parameters (with the same colors) marked in Fig. 11(b). The numerical results are presented by lines and the experimental results by markers.

constructed using a Generative Adversarial Network (GAN), which is trained using the data obtained from MCMC random walk.

For the conducted inference, it appears that the material model fed by the MCMC or synthetic realizations can reproduce the different loading cases, and in particular can discriminate between tension and compression, on the one hand in the visco-elastic range through a Poisson's ratio evolving with time, and on the other hand in the visco-plastic range through different hardening curves in tension and compression combined to a pressure sensitive yield surface.

Since the SBI was conducted for PA12 samples printed along two directions, the inferred parameters have different statistical properties for these two directions as well. In the future an anisotropic VE-VP model should be considered in order to have a model that can be applied for complex printed structures.

Acknowledgment

This project has received funding from the European Union's Horizon 2020 research and innovation programme under grant agreement No 862015 for the project "Multi-scale Optimisation for Additive Manufacturing of fatigue resistant shock-absorbing MetaMaterials (MOAMMM)" of the H2020-EU.1.2.1. - FET Open Programme.

Data availability

The raw/processed data required to reproduce these findings as well as the BI code and GAN generator are available on 'https://gitlab.uliege.be/moammm/moammmpublic/publicationsData/2023_BI_PA12' under the Creative Commons Attribution 4.0 International (CC BY 4.0) licence and under the stabilized version [44].

Appendix A. The experimental observations of the "H" PA12 specimens

In Fig. A.14, the marked points are the strain-stress pairs of experimental observations used in the BI for the "H" specimens.

Appendix B. Gaussian kernel-density estimation

The given data-set $\boldsymbol{\vartheta}_i$, $(i = 1, ..., N)$, serves as N realizations of a random vector $\boldsymbol{\Theta}$ with value in $\mathbb{R}^{N_\mathrm{p}}$. The data-set is first normalized by removing the mean and scaling it to the unit variance using a Principal Component Analysis, yielding a data set $\boldsymbol{\eta}_i$, $(i = 1, ..., N)$, which serves as N realizations of a random vector $\mathbf{H}$ with value in $\mathbb{R}^{N_\mathrm{p}}$. The non-parametric estimate of the probability distribution function (pdf) $\pi_{\mathbf{H}}$ can be constructed by using the Gaussian kernel-density estimation method, with

$$\pi_{\mathbf{H}}(\boldsymbol{\eta}) = \frac{1}{N}\sum_{i=1}^{N} \frac{1}{\left(\sqrt{2\pi}\hat{s}_{N_\mathrm{p}}\right)^{N_\mathrm{p}}} \exp\left(-\frac{1}{2\hat{s}_{N_\mathrm{p}}^2}\left\|\frac{\hat{s}_{N_\mathrm{p}}}{s_{N_\mathrm{p}}}\boldsymbol{\eta}_i - \boldsymbol{\eta}\right\|^2\right), \tag{B.1}$$

with $\|\boldsymbol{\eta}\|^2 = \eta_1^2 + ... + \eta_{N_\mathrm{p}}^2$, and where the multidimensional optimal Silverman bandwith s_{N_p} and parameter $\hat{s}_{N_\mathrm{p}}$ read

$$s_{N_\mathrm{p}} = \left[\frac{4}{N\left(2+N_\mathrm{p}\right)}\right]^{1/(4+N_\mathrm{p})}, \text{ and } \quad \hat{s}_{N_\mathrm{p}} = \frac{s_{N_\mathrm{p}}}{\sqrt{s_{N_\mathrm{p}}^2 + \frac{N-1}{N}}}. \tag{B.2}$$

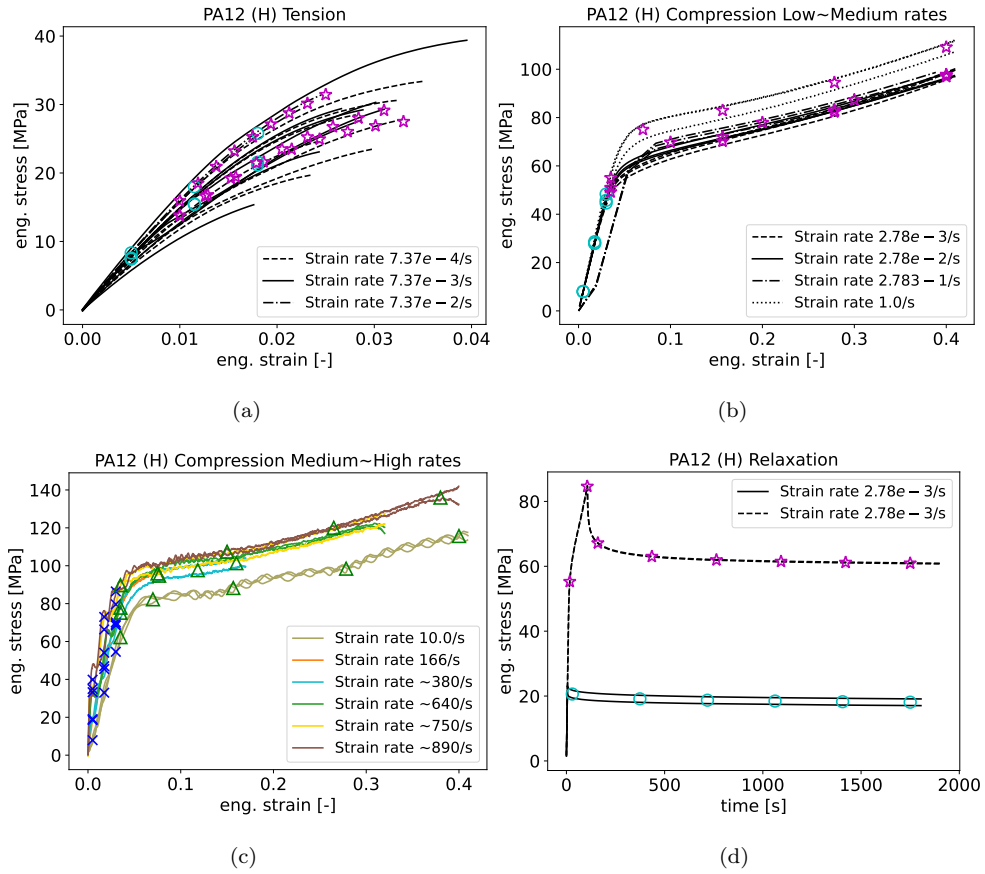

Figure A.14: The experimental strain-stress curves of the "H" specimens and the picked observation points to conduct the Bayesian inference in (a) Tension; (b) and (c) Compression at low, medium and high loading rates respectively; and (d) Compression and relaxation tests.

Appendix C. Joint and marginal distributions of material parameters

Appendix C.1. For the "V" specimens

For the material parameters identified on the "V" specimens, a part of the joint distributions is presented in Figs. C.15 by 2D histograms. The marginal distributions of all the 32 material parameters identified on the "V" specimens are presented in Fig. C.16 for the visco-elastic part and in Fig. C.17 for the visco-plastic part.

Appendix C.2. For the "H" specimens

For the material parameters identified on the "H" specimens, a part of the joint distributions is presented in Figs. C.15 by 2D histograms. The marginal distributions of all the 32 material parameters identified on the "H" specimens are presented in Fig. C.19 for the visco-elastic part and in Fig. C.20 for the visco-plastic part.

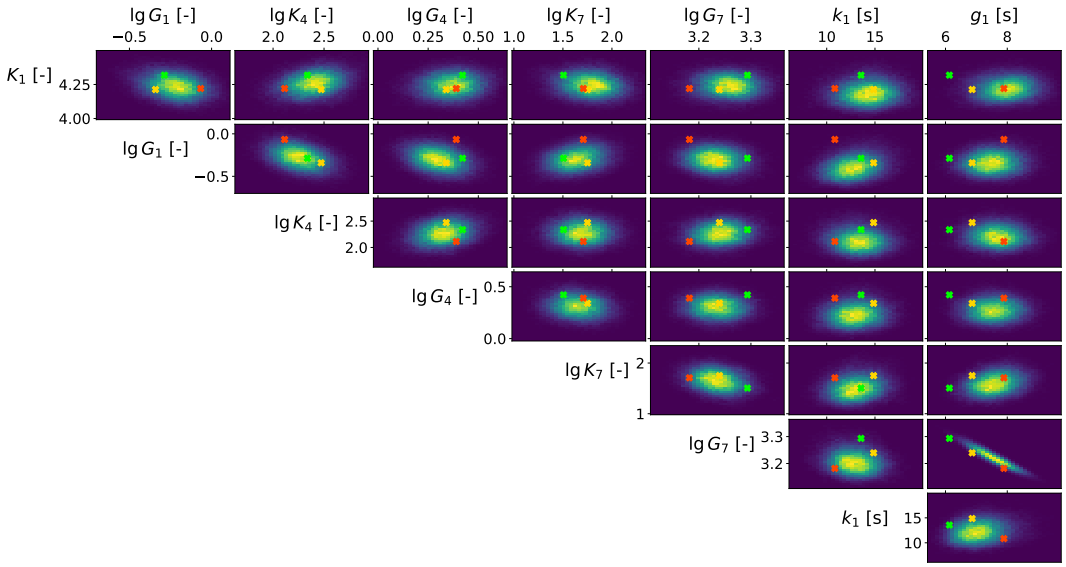

(a)

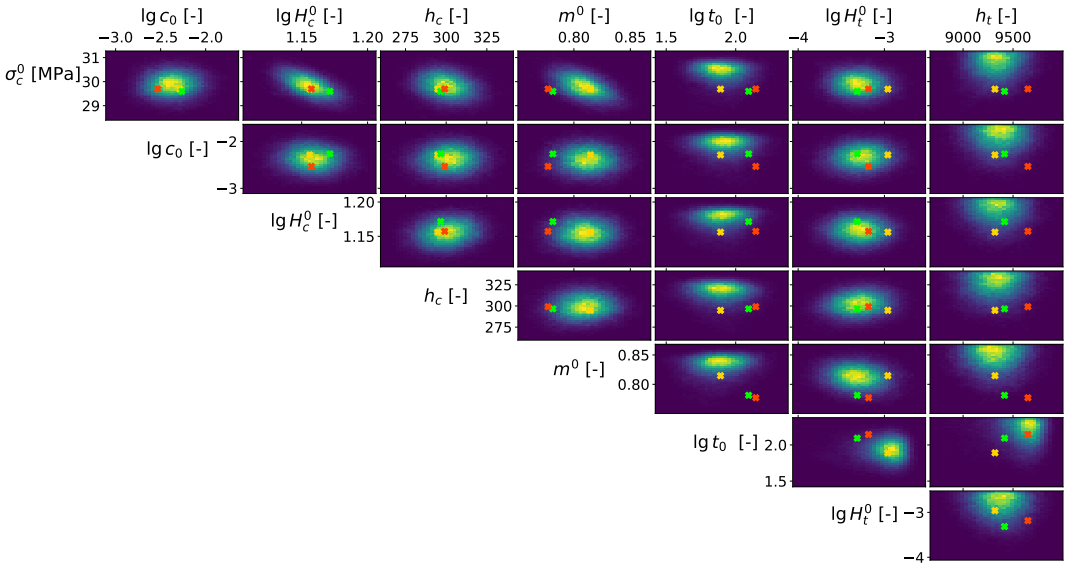

(b)

Figure C.15: The random material parameters distributions for the "V" specimens. The marked parameter points correspond to the numerical results (with the same colors) in Fig. 8. All the parameters in a logarithmic form are in the unit of MPa. Yellow and blue colors indicate respectively high and low probability density in the parameter space.

Appendix D. NNWs generated random material parameter

A part of joint distributions of the generated random parameters are presented by 2D histogram in Fig. D.21 for the "V" specimens, and in Fig. D.22 for "H" specimens.

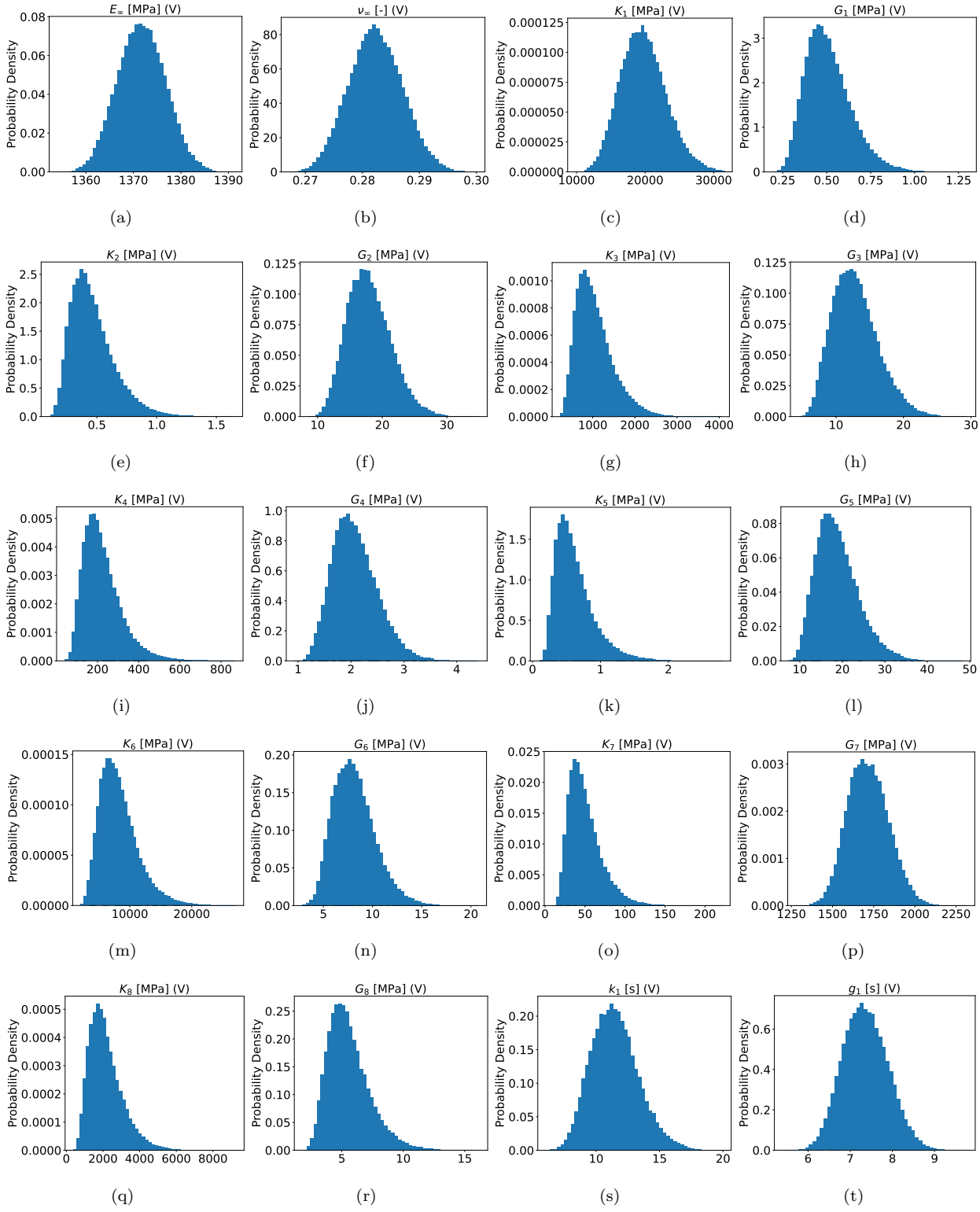

Figure C.16: Marginal distributions of identified visco-elastic material parameters for the “V” specimens.

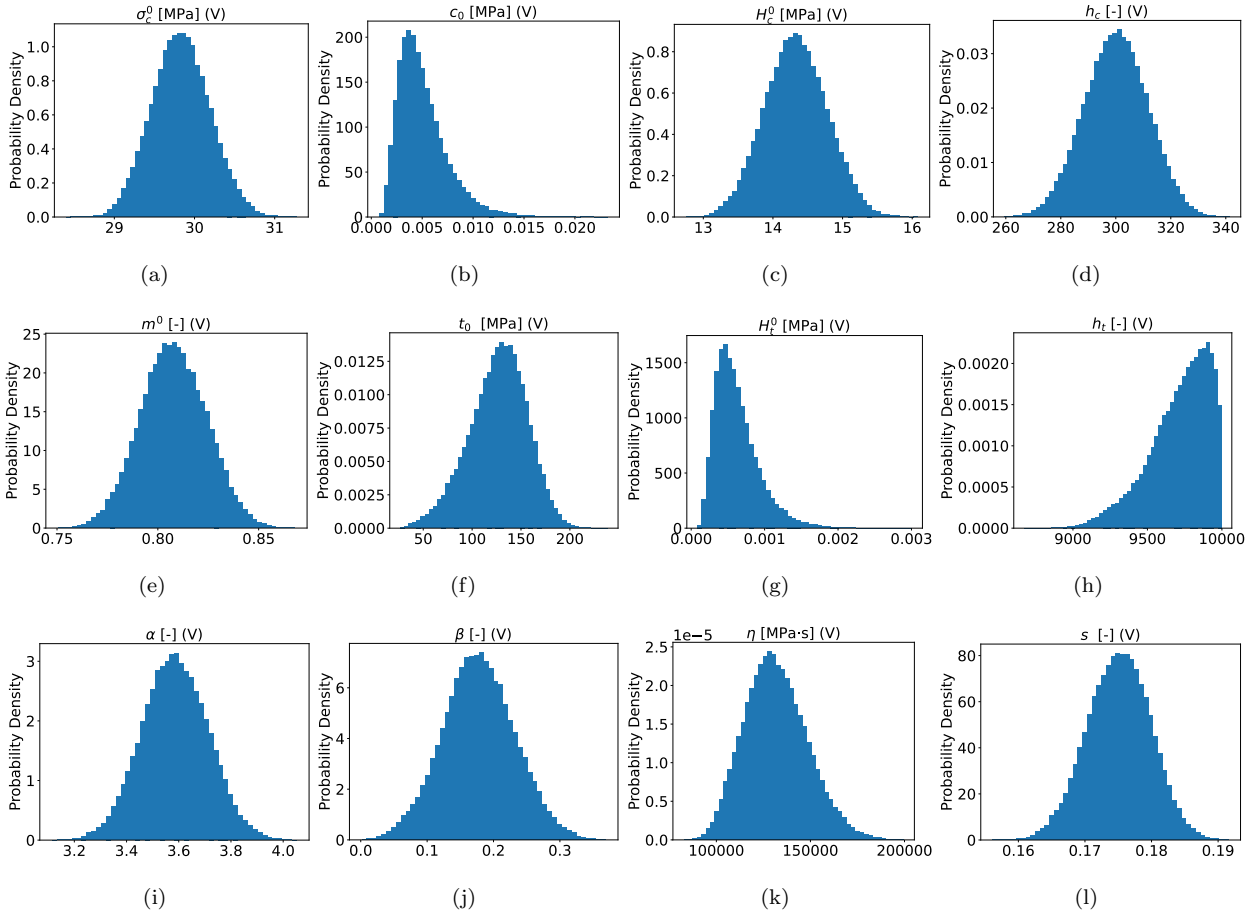

Figure C.17: Marginal distributions of identified visco-plastic material parameters for the “V” specimens.

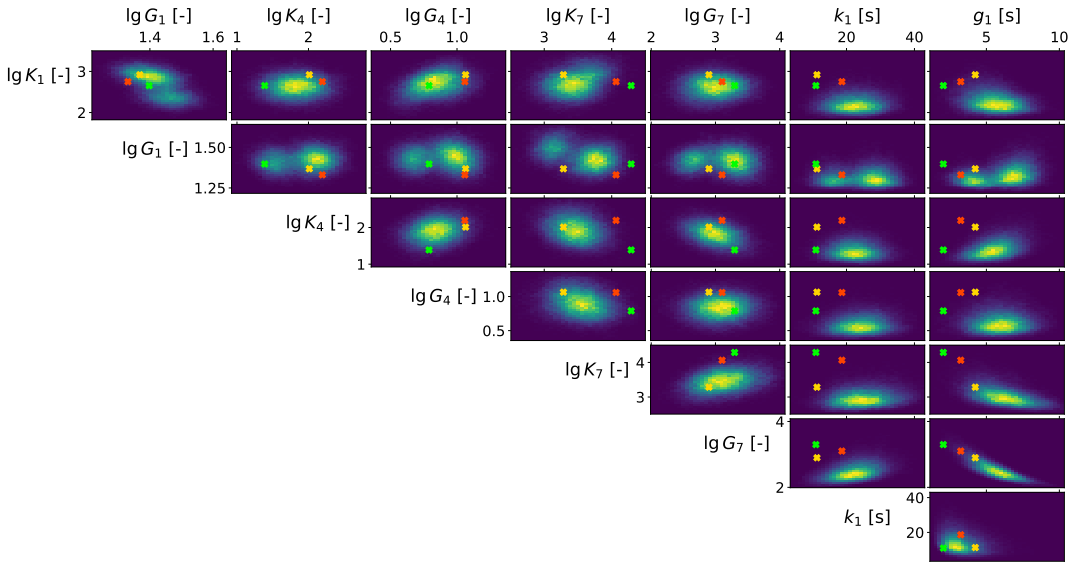

(a)

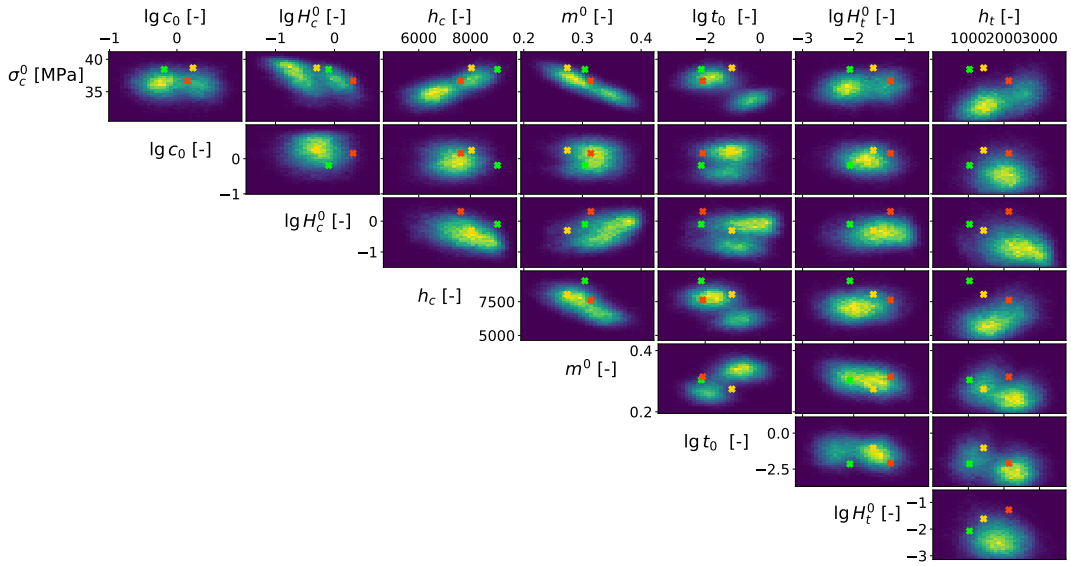

(b)

Figure C.18: The random material parameters distributions for the "H" specimens. The marked parameter points correspond to the numerical results (with the same colors) reported in Fig. 9. All the parameters in a logarithmic form are in the unit of MPa. Yellow and blue colors indicate respectively high and low probability density in the parameter space.

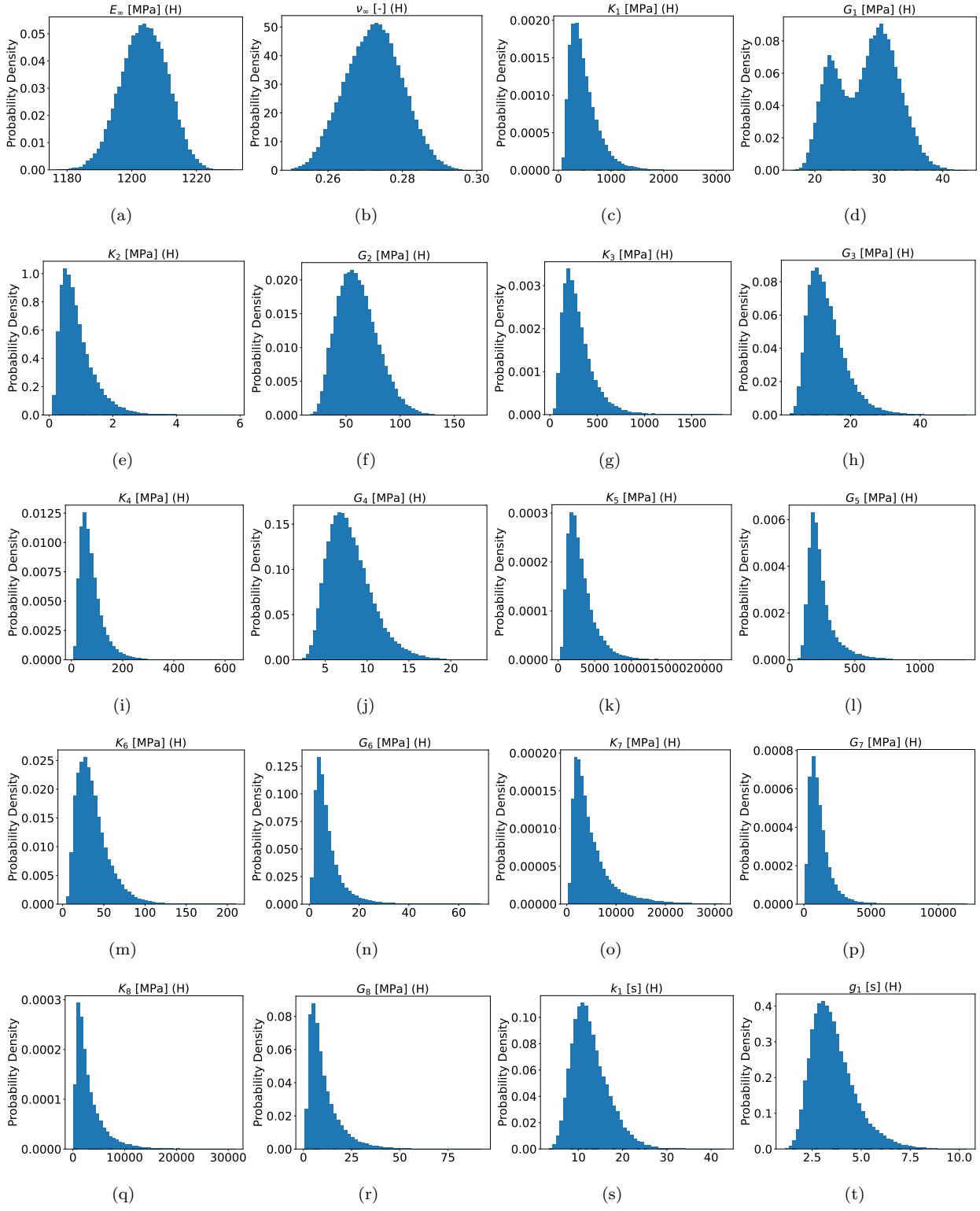

Figure C.19: Marginal distributions of identified visco-plastic material parameters for the “H” specimens.

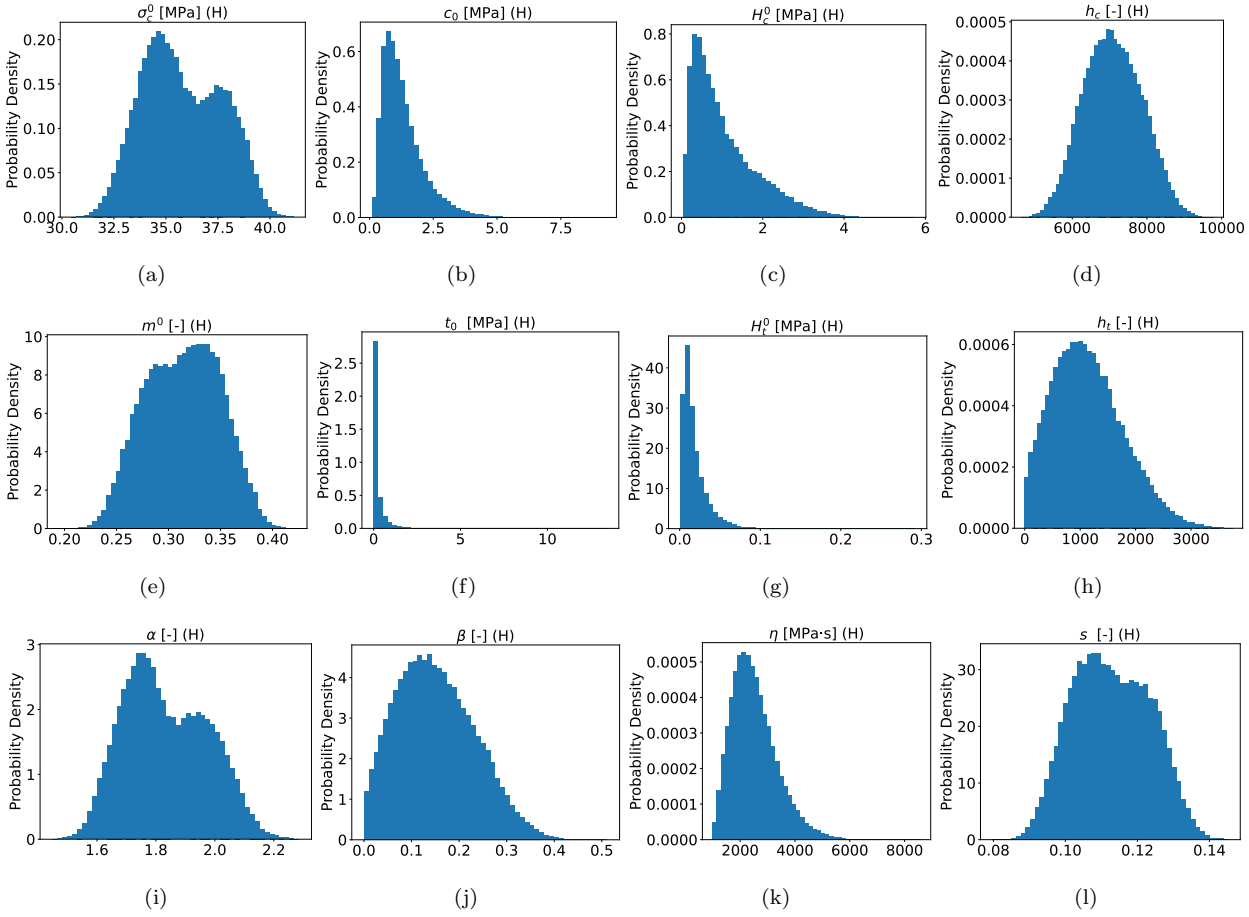

Figure C.20: Marginal distributions of identified visco-plastic material parameters for the "H" specimens.

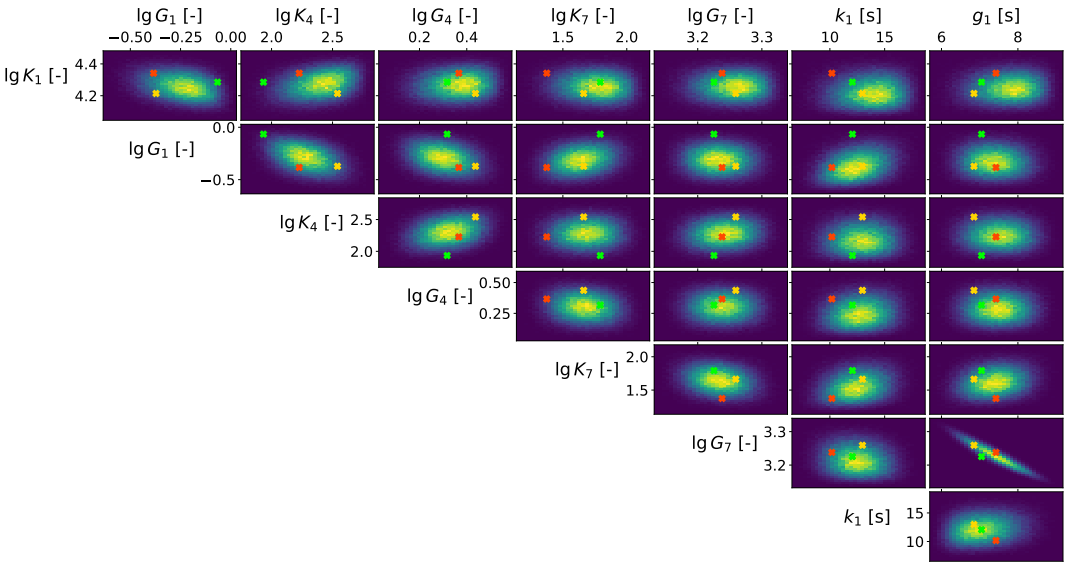

(a)

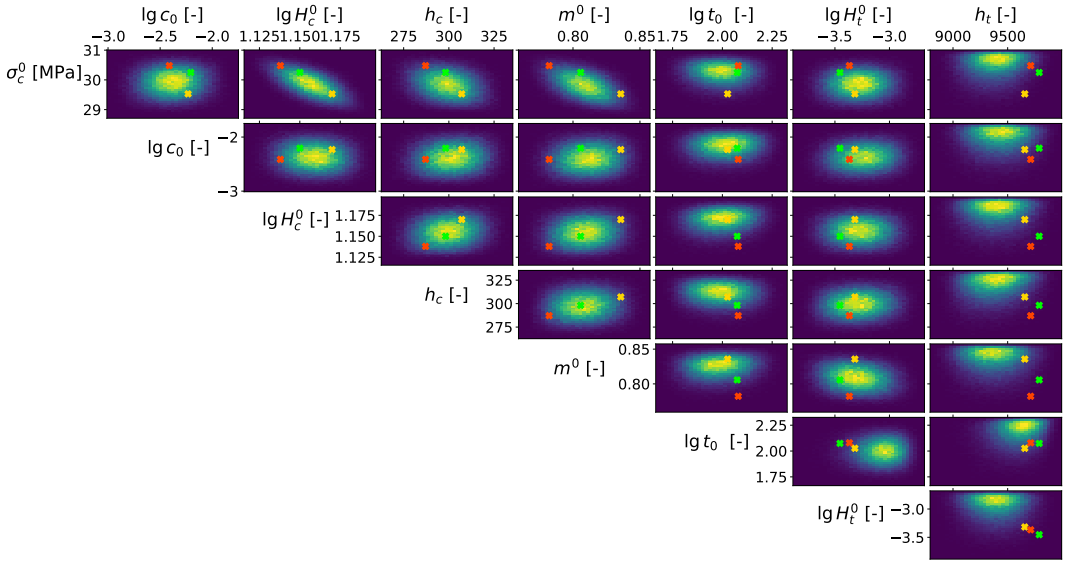

(b)

Figure D.21: The generated random material parameters distributions for the "V" specimens. The marked parameter points correspond to the numerical results (with the same colors) reported in Fig. 12. All the parameters in a logarithmic form are in the unit of MPa. Yellow and blue colors indicate respectively high and low probability density in the parameter space.

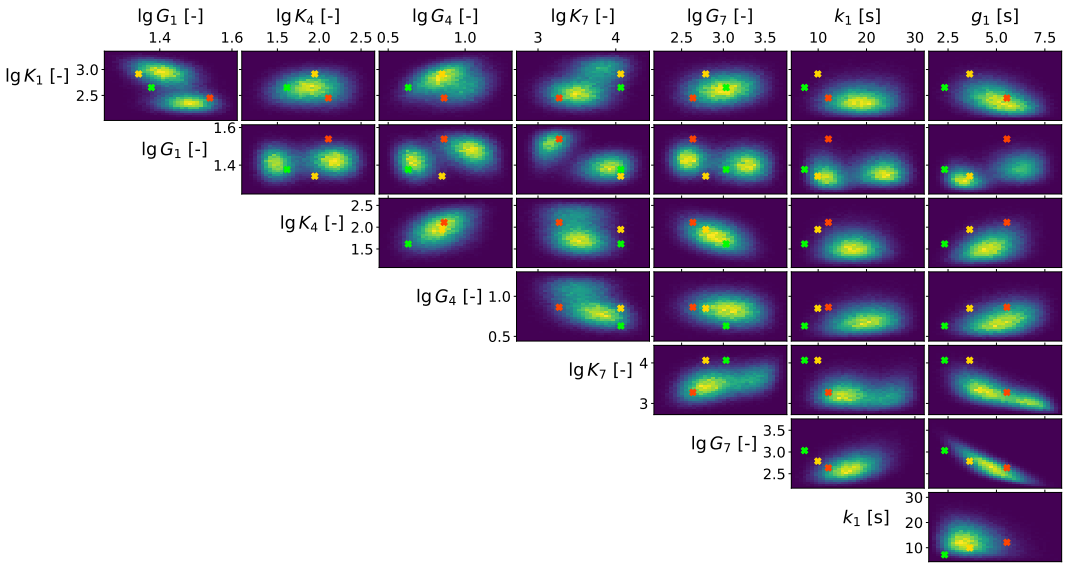

(a)

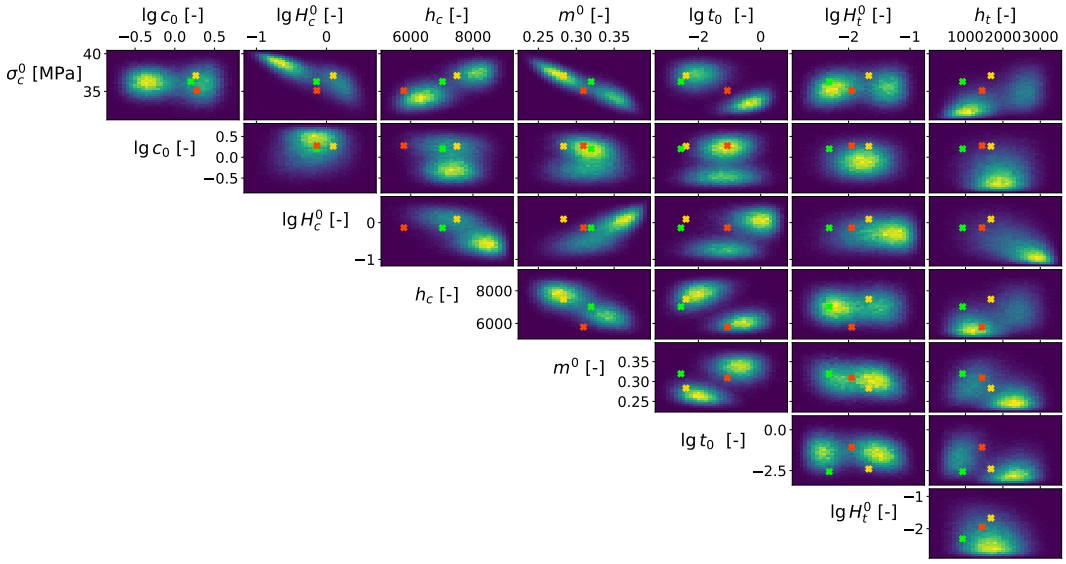

(b)

Figure D.22: The generated random material parameters distributions for the "H" specimens. The marked parameter points correspond to the numerical results (with the same colors) reported in Fig. 13. All the parameters in a logarithmic form are in the unit of MPa. Yellow and blue colors indicate respectively high and low probability density in the parameter space.

References

[1] D. L. Bourell, H. L. Marcus, J. W. Barlow, J. J. Beaman, Selective laser sintering of metals and ceramics, International Journal of Powder Metallurgy (Princeton, New Jersey) 28 (1992) 369 – 381. Cited by: 281.

[2] M. Chapiro, Current achievements and future outlook for composites in 3d printing, Reinforced Plastics 60 (2016) 372–375. URL: https://www.sciencedirect.com/science/article/pii/S0034361716303551. doi:https://doi.org/10.1016/j.repl.2016.10.002.

[3] R. Seltzer, F. M. de la Escalera, J. Segurado, Effect of water conditioning on the fracture behavior of pa12 composites processed by selective laser sintering, Materials Science and Engineering: A 528 (2011) 6927–6933.

[4] U. Ajoku, N. Saleh, N. Hopkinson, R. Hague, P. Erasenthiran, Investigating mechanical anisotropy and end-of-vector effect in laser-sintered nylon parts, Proceedings of the Institution of Mechanical Engineers, Part B: Journal of Engineering Manufacture 220 (2006) 1077–1086.

[5] S.-L. Sindinger, C. Kralovec, D. Tasch, M. Schagerl, Thickness dependent anisotropy of mechanical properties and inhomogeneous porosity characteristics in laser-sintered polyamide 12 specimens, Additive Manufacturing 33 (2020) 101141.

[6] T. L. Starr, T. J. Gornet, J. S. Usher, The effect of process conditions on mechanical properties of laser-sintered nylon, Rapid Prototyping Journale 17 (2011) 418–423.

[7] B. Caulfield, P. McHugh, S. Lohfeld, Dependence of mechanical properties of polyamide components on build parameters in the sls process, Journal of Materials Processing Technology 182 (2007) 477–488. URL: https://www.sciencedirect.com/science/article/pii/S0924013606007886. doi:https://doi.org/10.1016/j.jmatprotec.2006.09.007.

[8] M. Faes, Y. Wang, P. Lava, D. Moens, Variability in the mechanical properties of laser sintered pa-12 components, in: 2015 International Solid Freeform Fabrication Symposium, University of Texas at Austin, 2015.

[9] N. Lammens, M. Kersemans, I. De Baere, W. Van Paepegem, On the visco-elasto-plastic response of additively manufactured polyamide-12 (pa-12) through selective laser sintering, Polymer Testing 57 (2017) 149–155. URL: https://www.sciencedirect.com/science/article/pii/S0142941816310315. doi:https://doi.org/10.1016/j.polymertesting.2016.11.032.

[10] L. Cobian, M. Rueda-Ruiz, J. Fernandez-Blazquez, V. Martinez, F. Galvez, F. Karayagiz, T. Lück, J. Segurado, M. Monclus, Micromechanical characterization of the material response in a pa12-sls fabricated lattice structure and its correlation with bulk behavior, Polymer Testing 110 (2022) 107556. doi:https://doi.org/10.1016/j.polymertesting.2022.107556.

[11] J. Schneider, S. Kumar, Multiscale characterization and constitutive parameters identification of polyamide (pa12) processed via selective laser sintering, Polymer Testing 86 (2020) 106357. URL: https://www.sciencedirect.com/science/article/pii/S0142941819320860. doi:https://doi.org/10.1016/j.polymertesting.2020.106357.

[12] B. Miled, I. Doghri, L. Delannay, Coupled viscoelastic–viscoplastic modeling of homogeneous and isotropic polymers: Numerical algorithm and analytical solutions, Computer Methods in Applied Mechanics and Engineering 200 (2011) 3381–3394. URL: https://www.sciencedirect.com/science/article/pii/S0045782511002702. doi:https://doi.org/10.1016/j.cma.2011.08.015.

[13] J.-C. Simo, On a fully three-dimensional finite-strain viscoelastic damage model: Formulation and computational aspects, Computer Methods in Applied Mechanics and Engineering 60 (1987) 153–173. URL: https://www.sciencedirect.com/science/article/pii/0045782587901071. doi:https://doi.org/10.1016/0045-7825(87)90107-1.

[14] P. Perzyna, Thermodynamic theory of viscoplasticity, volume 11 of *Advances in Applied Mechanics*, Elsevier, 1971, pp. 313–354. URL: https://www.sciencedirect.com/science/article/pii/S0065215608703454. doi:https://doi.org/10.1016/S0065-2156(08)70345-4.

[15] V.-D. Nguyen, F. Lani, T. Pardoen, X. Morelle, L. Noels, A large strain hyperelastic viscoelastic-viscoplastic-damage constitutive model based on a multi-mechanism non-local damage continuum for amorphous glassy polymers, Interna-

tional Journal of Solids and Structures 96 (2016) 192–216. URL: https://www.sciencedirect.com/science/article/pii/S0020768316301238. doi:https://doi.org/10.1016/j.ijsolstr.2016.06.008.

[16] J. D. Ferry, Viscoelastic properties of polymers, John Wiley & Sons, 1980.

[17] J. Isenberg, Progressing from least squares to bayesian estimation, in: ASME (Ed.), Proceedings of the 1979 ASME design engineering technical conference, New York, USA, 1979, pp. 71–82.

[18] J. L. Beck, L. S. Katafygiotis, Updating models and their uncertainties. I: Bayesian statistical framework, Journal of Engineering Mechanics 124 (1998) 455–461.

[19] T. Most, Identification of the parameters of complex constitutive models: Least squares minimization vs. bayesian updating, in: D. Straub (Ed.), Reliability and Optimization of Structural Systems, 2010.

[20] H. Rappel, L. Beex, L. Noels, S. Bordas, Identifying elastoplastic parameters with bayes' theorem considering output error, input error and model uncertainty, Probabilistic Engineering Mechanics 55 (2019) 28 – 41. doi:10.1016/j.probengmech.2018.08.004.

[21] H. Rappel, L. Beex, J. Hale, L. Noels, S. Bordas, A tutorial on bayesian inference to identify material parameters in solid mechanics, Archives of Computational Methods in Engineering (2019). doi:10.1007/s11831-018-09311-x.

[22] Z. Chen, P. Jin, R. Li, Y. Qi, G. Cai, Parameter identification of elastoplastic model for cucrzr alloy by the neural network-aided bayesian inference, Fatigue & Fracture of Engineering Materials & Structures n/a (????) n/a. URL: https://onlinelibrary.wiley.com/doi/abs/10.1111/ffe.14000. doi:https://doi.org/10.1111/ffe.14000. arXiv:https://onlinelibrary.wiley.com/doi/pdf/10.1111/ffe.14000.

[23] W. Hernandez, F. Borges, D. Castello, N. Roitman, C. Magluta, Bayesian inference applied on model calibration of a fractional derivative viscoelastic model, in: DINAME 2015 - Proceedings of the XVII International Symposium on Dynamic Problems of Mechanics, 2015.

[24] H. Rappel, L. A. A. Beex, S. P. A. Bordas, Bayesian inference to identify parameters in viscoelasticity, Mechanics of Time-Dependent Materials 22 (2018) 221–258. doi:10.1007/s11043-017-9361-0.

[25] S. Madireddy, B. Sista, K. Vemaganti, A bayesian approach to selecting hyperelastic constitutive models of soft tissue, Computer Methods in Applied Mechanics and Engineering 291 (2015) 102 – 122. doi:10.1016/j.cma.2015.03.012.

[26] J. L. de Pablos, I. Sabirov, I. Romero, An experimental, computational, and statistical strategy for the bayesian calibration of complex material models, Archives of Computational Methods in Engineering (2023). URL: https://doi.org/10.1007/s11831-023-09888-. doi:https://doi.org/10.1007/s11831-023-09888-y.

[27] M. J. Bogdanor, S. Mahadevan, C. Oskay, Uncertainty quantification in damage modeling of heterogeneous materials, International Journal for Multiscale Computational Engineering 11 (2013) 289–307. doi:10.1615/IntJMultCompEng.2013005821.

[28] M. J. Bogdanor, C. Oskay, S. B. Clay, Multiscale modeling of failure in composites under model parameter uncertainty, Computational Mechanics 56 (2015) 389–404. doi:10.1007/s00466-015-1177-7.

[29] M. Mohamedou, K. Z. Uriondo, C. N. Chung, H. Rappel, L. Beex, L. Adam, Z. Major, L. Wu, L. Noels, Bayesian identification of mean-field homogenization model parameters and uncertain matrix behavior in non-aligned short fiber composites, Composite Structures Submitted (2019).

[30] L. Wu, K. Zulueta, Z. Major, A. Arriaga, L. Noels, Bayesian inference of non-linear multiscale model parameters accelerated by a deep neural network, Computer Methods in Applied Mechanics and Engineering 360 (2020) 112693. URL: https://www.sciencedirect.com/science/article/pii/S004578251930578X. doi:https://doi.org/10.1016/j.cma.2019.112693.

[31] B. Georgios, K. Benedikt, R. Raimund, Data-driven inverse uncertainty quantification in the transverse tensile response of carbon fiber reinforced composites, Composites Science and Technology 211 (2021) 108845. URL: https://www.sciencedirect.com/science/article/pii/S0266353821002013. doi:https://doi.org/10.1016/j.compscitech.2021.108845.

[32] P.-S. Koutsourelakis, A novel bayesian strategy for the identification of spatially varying material properties and model

validation: an application to static elastography, International Journal for Numerical Methods in Engineering 91 (2012) 249–268. doi:10.1002/nme.4261.

[33] A. Vigliotti, G. Csányi, V. Deshpande, Bayesian inference of the spatial distributions of material properties, Journal of the Mechanics and Physics of Solids 118 (2018) 74 – 97. doi:10.1016/j.jmps.2018.05.007.

[34] H. M. Paranjape, K. I. Aycock, C. Bonsignore, J. D. Weaver, B. A. Craven, T. W. Duerig, A probabilistic approach with built-in uncertainty quantification for the calibration of a superelastic constitutive model from full-field strain data, Computational Materials Science 192 (2021) 110357. URL: https://www.sciencedirect.com/science/article/pii/S0927025621000823. doi:https://doi.org/10.1016/j.commatsci.2021.110357.

[35] C. Soize, R. Ghanem, Data-driven probability concentration and sampling on manifold, Journal of Computational Physics 321 (2016) 242–258. URL: https://www.sciencedirect.com/science/article/pii/S0021999116301899. doi:https://doi.org/10.1016/j.jcp.2016.05.044.

[36] L. Wu, V.-D. Nguyen, L. Adam, L. Noels, An inverse micro-mechanical analysis toward the stochastic homogenization of nonlinear random composites, Computer Methods in Applied Mechanics and Engineering 348 (2019) 97–138. URL: https://www.sciencedirect.com/science/article/pii/S0045782519300210. doi:https://doi.org/10.1016/j.cma.2019.01.016.

[37] B. Moran, M. Ortiz, C. F. Shih, Formulation of implicit finite element methods for multiplicative finite deformation plasticity, International Journal for Numerical Methods in Engineering 29 (1990) 483–514. URL: https://onlinelibrary.wiley.com/doi/abs/10.1002/nme.1620290304. doi:https://doi.org/10.1002/nme.1620290304. arXiv:https://onlinelibrary.wiley.com/doi/pdf/10.1002/nme.1620290304.

[38] A. Melro, P. Camanho, F. Andrade Pires, S. Pinho, Micromechanical analysis of polymer composites reinforced by unidirectional fibres: Part i – constitutive modelling, International Journal of Solids and Structures 50 (2013) 1897–1905. URL: https://www.sciencedirect.com/science/article/pii/S0020768313000747. doi:https://doi.org/10.1016/j.ijsolstr.2013.02.009.

[39] C. M. Bishop, in: Pattern Recognition and Machine Learning, Information Science and Statistics, Springer-Verlag, New York, USA, 2006.

[40] I. M. Ward, Determination of molecular orientation by spectroscopic techniques, in: H. H. Kaush, H. G. Zachman (Eds.), Characterization of Polymers in the Solid State I: Part A: NMR and Other Spectroscopic Methods Part B: Mechanical Methods, Springer Berlin Heidelberg, Berlin, Heidelberg, 1985, pp. 81–115.

[41] R. N. Haward, The physics of glassy polymers, Springer Science & Business Media, 2012.

[42] H. Haario, E. Saksman, J. Tamminen, Adaptive proposal distribution for random walk metropolis algorithm, Computational Statistics 14 (1999) 375–395. doi:10.1007/s001800050022.

[43] W. Gilks, S. Richardson, D. Spiegelhalter, Markov chain monte carlo in practice, in: Chapman & Hall/CRC Interdisciplinary Statistic, Chapman and Hall, Weinheim, Germany, 1995.

[44] L. Wu, C. Anglade, L. Cobian, M. Monclus, J. Segurado, F. Karayagiz, U. Freitas, L. Noels, Data of "Bayesian inference of high-dimensional finite-strain visco-elastic-visco-plastic model parameters for additive manufactured polymers and neural network based material parameters generator", 2023. URL: https://doi.org/10.5281/zenodo.7792804. doi:10.5281/zenodo.7792804.